A Triiron Complex with *N*-Ferrocenyl Aminocarbyne Ligand Bridging a Diiron Core: DFT, Electrochemical and Biological Insights

Chiara Saviozzi,[a] Lorenzo Biancalana,[a] Tiziana Funaioli,[a] Marco Bortoluzzi,[b] Michele De Franco,[c] Massimo Guelfi,[a] Valentina Gandin,[c] Fabio Marchetti [a,*]

[a] University of Pisa, Department of Chemistry and Industrial Chemistry, Via G. Moruzzi 13, I-56124 Pisa, Italy.

[b] University of Venezia "Ca' Foscari", Department of Molecular Science and Nanosystems, Via Torino 155, I-30170 Mestre (VE), Italy.

[c] University of Padova, Department of Pharmaceutical and Pharmacological Sciences, Via F. Marzolo 5, I-35131 Padova, Italy.

Corresponding Author

[*]E-mail address: fabio.marchetti@unipi.it

Webpage: https://people.unipi.it/fabio_marchetti/

Abstract

The first *N*-ferrocenyl aminocarbyne complex, $[Fe_2Cp_2(CO)_2(\mu\text{-}CO)\{\mu\text{-}CN(Me)(Fc)\}]CF_3SO_3$ (**[2]CF_3SO_3**), was synthesized with an 88% yield from $[Fe_2Cp_2(CO)_4]$, isocyanoferrocene (CNFc) and methyl triflate. The synthesis proceeded through the intermediate formation of $[Fe_2Cp_2(CO)_3(CNFc)]$, **1**. Multinuclear NMR experiments revealed the presence of *cis* and *trans* isomers for **[2]CF_3SO_3** in organic solvents, in agreement with DFT outcomes. Electrochemical and spectroelectrochemical studies demonstrated one reduction process occurring prevalently at the diiron core, and one oxidation involving the ferrocenyl substituent. The oxidation process is expected to favor the redox activation of **[2]**$^+$ in a biological environment. Both **[2]CF_3SO_3** and its phenyl analogue $[Fe_2Cp_2(CO)_2(\mu\text{-}CO)\{\mu\text{-}CN(Me)(Ph)\}]CF_3SO_3$ (**[3]CF_3SO_3**), prepared for comparison, exerted moderate antiproliferative activity against the human cancer cell lines A431, HCT-15, PSN-1, 2008 and U1285. However, **[2]CF_3SO_3** exhibited a higher cytotoxicity than **[3]CF_3SO_3**, showed a substantial ability to induce intracellular ROS production, and outperformed cisplatin in a three-dimensional SCLC cell model.

Keywords: bioorganometallic chemistry; isocyanoferrocene; diiron complexes; metal-metal cooperativity; anticancer metal drugs; 3D cell models.

Introduction

The ferrocene skeleton ($FeCp_2$, Cp = η^5-C_5H_5) possesses unique redox behavior, low toxicity and outstanding stability, and these properties have stimulated research in diverse fields.[1,2,3] In particular, the ferrocene scaffold has garnered significant attention for formulating new anticancer metallodrugs.[4,5] Ferrocenyl compounds typically exert their antiproliferative activity by undergoing Fe^{II} to Fe^{III} oxidation in the tumor environment; this electron transfer disrupts cellular redox homeostasis, ultimately leading to cell death.[6,7] To harness the beneficial characteristics of ferrocene and create synergistic effects, synthetic chemists have pursued conjugation strategies. Basically, these strategies

involve modifying one or two cyclopentadienyl rings of $FeCp_2$ with suitable functionalities (*e.g.*, phosphine groups, tetradentate Schiff bases, NHC carbenes), capable of binding to another metal center.[8,9] Concerning potential medicinal applications, various metal structures with documented biological activities have been attached to ferrocene. Examples include ruthenium(III) complexes analogous to NAMI-A,[10] platinum(II) complexes,[11,12] and Ru(II) arene complexes (Figure 1).[13,14,15]

Expanding the nuclearity of iron complexes by introducing the ferrocenyl unit can potentially enhance the properties and robustness of the resulting polyiron structures when compared to their lower nuclearity counterparts.[16,17] In particular, having iron centers in distinct oxidation states may open up multiple redox pathways. For example, attaching a phosphino-ferrocene ligand to a diiron carbonyl core, serving as a model for the active site of [FeFe]-hydrogenases, was previously found to optimize the redox catalytic performance of the resulting mixed valence triiron complex.[18] Interestingly, despite its potential, this approach has been under-explored in the field of medicinal chemistry.

The commercially available compound $[Fe_2Cp_2(CO)_4]$ offers an excellent platform for investigating novel reactivity patterns, due to its cost-effectiveness and the cooperative effects that arise from the two adjacent metal centers.[19,20,21] Two primary classes of derivatives of $[Fe_2Cp_2(CO)_4]$, featuring a bridging cationic ligand, can be readily obtained through the sequential assembly of an isocyanide, an alkyl cation and an alkyne (Figure 1, structures **I** and **II**).[22] These two families of diiron compounds possess a rare combination of desirable pre-requisites for medicinal applications, including a straightforward synthetic procedure, extended structural variability, adequate water solubility enhanced by their ionic nature, and substantial stability in aqueous media.[23] We recently unveiled the promising anticancer potential of selected compounds of types **I** [24] and **II**.[25,26,27] Additionally, we discovered that the incorporation of the ferrocenyl moiety within **II** using alkynyl ferrocene, $CpFe(\eta^5\text{-}C_5H_4C{\equiv}CH)$, enhances the antiproliferative activity of the resulting complexes (Figure 1, structure **III**) compared to ferrocenyl lacking analogs.[28]

Building on this premise, we became interested in incorporating the ferrocenyl unit as a substituent of the compact amino-alkylidyne (aminocarbyne[29]) group in **I**. It is noteworthy that, while complexes **I** are normally indefinitely air-stable and robust in a wide range of solvents (including aqueous media), their stability might be sensibly reduced with certain nitrogen substituents (R, R') bearing unfavorable electronic properties (e.g., acetyl/benzoyl groups) or steric bulkiness (tert-butyl).[22,30,31]

Adding a suitable electrophile to a pre-existing isocyanide ligand (M-CNR) represents the most common literature strategy for obtaining aminocarbyne ligands (M-CNRR').[22,32] Accordingly, the typical synthesis of **I** involves the initial reaction of $[Fe_2Cp_2(CO)_4]$ with an isocyanide, followed by N-alkylation.[33]

Isocyanoferrocene (CNFc) is the simplest isocyanide-decorated ferrocene, and its utilization in coordination chemistry has been relatively limited, possibly due to its commercial unavailability and the challenging and tedious synthesis.[34] Specifically, examples of isocyanoferrocene coordination to metal centers have been substantially limited to ruthenium,[35] iron phthalocyanine,[36] diiron thiolate[37] and chromium complexes, including the unique case of a homoleptic isocyanoferrocene complex, *i.e.* $[Cr(CNFc)_6]$.[38] The scarce development of this topic is underscored by the observation that chemical modification of the isocyanoferrocene ligand has been mostly confined to gold complexes, where amine addition to coordinated CNFc resulted in its conversion into diamino-alkylidene.[39]

The scarcity of information in this context sharply contrasts with the extensive use of isocyanides as universal and versatile ligands in coordination chemistry.[40,41]

In this work, we introduce isocyanoferrocene (for which an optimized synthesis is provided) as a ligand to the $\{Fe_2Cp_2(CO)_3\}$ framework, and its unprecedented transformation into an aminocarbyne ligand. The overall assembly can be viewed as a triiron system consisting of a Fe^{II} center (ferrocenyl) and a Fe^{I}-Fe^{I} dinuclear core. We present the structural and electrochemical characterization of the resulting triiron complex, along with a preliminary evaluation of the anticancer potential in both 2D and 3D cell models.

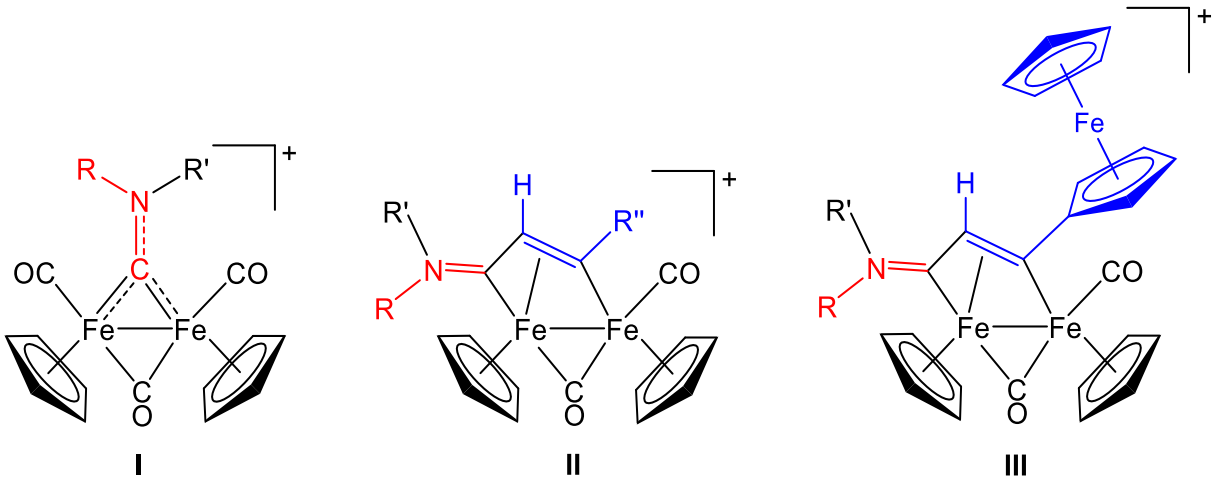

Figure 1. General structures of diiron aminocarbyne complexes (**I**) derived from $[Fe_2Cp_2(CO)_4]$, an isocyanide (CNR, red) and an alkylating agent (R'); their vinyliminium derivatives (**II**) resulting from the incorporation of an alkyne (HC≡CR'', blue); including the case of HC≡CFc (**III**). $CF_3SO_3^-$ or BF_4^- salts. R, R' = alkyl/aryl groups; R'' = H, alkyl, aryl, pyridyl, thiophenyl, carboxylate, $SiMe_3$.

Results and discussion

1. Synthesis, spectroscopic characterization and DFT analysis.

Initially, isocyanoferrocene, CNFc, was synthesized from ferrocene via the intermediate formation of aminoferrocene, using a multistep procedure optimized with respect to the literature (for details, refer to the Experimental section and the Supporting Information). Subsequently, the reaction between $[Fe_2Cp_2(CO)_4]$ and freshly prepared CNFc, in a 1:1 molar ratio, was conducted in acetonitrile at room temperature and proceeded with the selective substitution of one carbonyl ligand with CNFc (Scheme 1). This aspect is nontrivial, as it is documented that allowing $[Fe_2Cp_2(CO)_4]$ to react with one equivalent of isocyanides can lead to multiple CO-CNR substitutions, resulting in mixtures of products.[33]

Based on infrared spectroscopy measurements, $[Fe_2Cp_2(CO)_3(CNFc)]$, **1** – an uncommon example of isocyanoferrocene coordination complex (see Introduction) – is believed to exist in solution as a mixture of four interconverting isomers. These isomers vary in the relative orientation of the Cp ligands (*cis* or *trans*) and the coordination site of the CNFc ligand (terminal or bridging), see Figure S3. This

situation aligns with the general case of $[Fe_2Cp_2(CO)_3(CNR)]$ complexes (R = alkyl or aryl).[33,42,43] Exception arising when bulkier R groups (*e.g.,* 2,6-dimethylphenyl and cyclohexyl) are present, disfavoring the bridging CNR coordination.[33] The interconversion of isomers in solution was previously elucidated to follow the Adams-Cotton mechanism, which entails the formation of bridge-opened intermediates (comprising only terminal ligands bound to the diiron core), where rotation around the Fe-Fe bond is permitted.[33,44]

In the case of **1**, *cis* and *trans* isomers display the IR bands accounting for the terminal CO ligands at 1988 and 1951 cm^{-1}, respectively (CH_2Cl_2 solution). Prior research has demonstrated that the isomeric composition of $[Fe_2Cp_2(CO)_3(CNR)]$ complexes is usually solvent-dependent, with polar solvents favoring the more polar *cis* isomer over the *trans* isomer.[45] In agreement with this observation, both *cis*-**1** and *trans*-**1** were detected in comparable amounts in CH_2Cl_2 (μ = 1.60 D) solution, while *cis*-**1** was prevalent in MeCN (μ = 3.92 D), Figure S4. The coordination mode of the CNFc ligand in **1** can be deduced from the corresponding CN stretching vibration, appearing at 2100 and 1691 cm^{-1} for terminal (C≡N) and bridging (C=N) coordination, respectively.[33,46] A comparative analysis of IR spectra suggests that the bridging-isocyanide isomers are slightly favored in acetonitrile solution compared to dichloromethane (Figures S3-S4). The wavenumber associated with the terminal CNFc is lower than that of non-coordinated CNFc (2122 cm^{-1} in CH_2Cl_2 solution), indicating a significant occurrence of Fe $\rightarrow$ CNFc π-back-donation in **1**.[33,42]

The crude solid residue obtained from $[Fe_2Cp_2(CO)_4]$ and CNFc was dissolved in dichloromethane and treated with methyl triflate, yielding the *N*-ferrocenyl aminocarbyne complex **[2]CF_3SO_3**. Notably, **[2]CF_3SO_3** could be purified through alumina chromatography without decomposition,[31] and was isolated as an air-stable red solid in 88 % yield (Scheme 1).

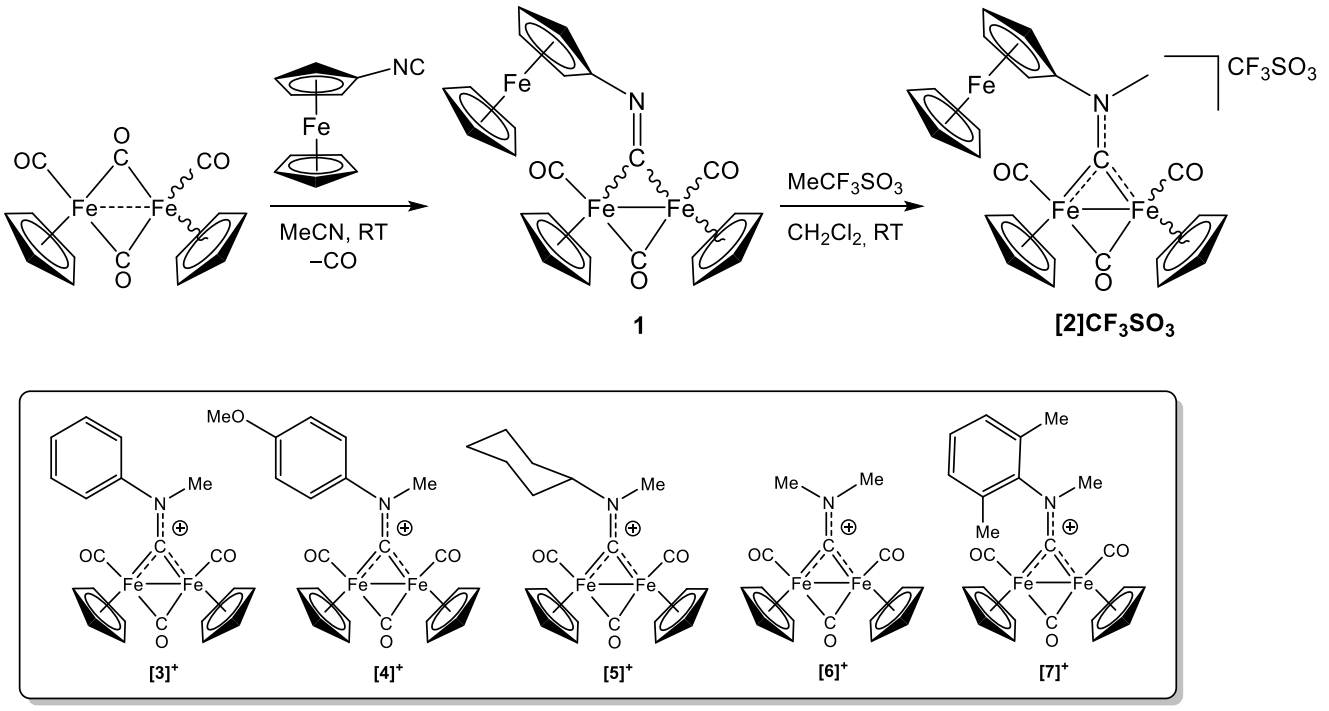

Scheme 1. Two-step synthesis of *N*-ferrocenyl aminocarbyne diiron complex **[2]CF_3SO_3** via intermediate formation of an isocyanoferrocene adduct (**1**). The presence of isomeric forms is indicated with wavy bonds; the structures of the isomers of **1** are shown in Figure S3. Inset: related diiron aminocarbyne complexes (triflate salts) employed and/or discussed in this work; [**3**]$^+$ is reported here for the first time, while [**4**]$^+$,[24] [**5**]$^+$,[24] [**6**]$^+$ [47] and [**7**]$^+$ [47] were previously described.

The ^{1}H NMR spectrum of **[2]CF_3SO_3** in $CDCl_3$ revealed the presence of two sets of signals in approximately 5:1 ratio, which were assigned to *cis* and *trans* isomers, respectively, based on NOESY evidence (Figures S6, S7 and S9). It is noteworthy that *cis*-*trans* isomerism has been rarely observed in diiron compounds of the type $[Fe_2Cp_2(CO)_2(\mu\text{-}CO)\{\mu\text{-}CN(R)(R')\}]^+$, and specifically only for R = R' = Me or Et.[48]

DFT calculations conducted on **[2]**$^+$ (PBEh-3c method, $CHCl_3$ as continuous medium) pointed out that the *cis* isomer is more stable than the *trans* one by 1.4 kcal/mol. This energy difference corresponds to a predicted *cis*/*trans* ratio of ≈11, at 298 K. The DFT optimized geometries of ***cis*-[2]**$^+$ and ***trans*-[2]**$^+$ are shown in Figure 2, and the most salient calculated bonding parameters are provided in the caption.

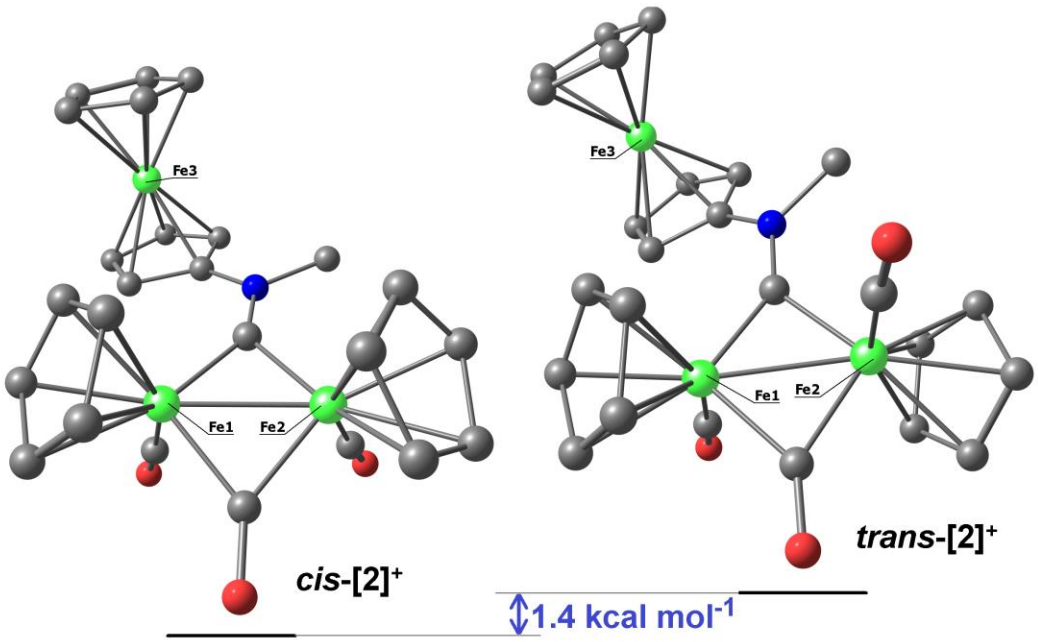

Figure 2. DFT optimized geometries of ***cis*-[2]**$^+$ (left) and ***trans*-[2]**$^+$ (right), computed at PBEh-3c level ($CHCl_3$ as continuous medium). Fe, green; N, blue; C, grey. Hydrogen atoms were omitted for clarity. Selected computed bond lengths for ***cis*-[2]**$^+$ (Å): Fe1-C(carbyne) 1.856; Fe2-C(carbyne) 1.894; carbyne-N 1.297; Fe1-Fe2 2.482; Fe1-C(CO) 1.776; Fe2-C(CO) 1.774; Fe1-C(μ-CO) 1.935; Fe2-C(μ-CO) 1.893; average Fe1-C(Cp) 2.112; average Fe2-C(Cp) 2.115; average Fe3-C(Cp) 2.058. Selected computed bond lengths for ***trans*-[2]**$^+$ (Å): Fe1-C(carbyne) 1.841; Fe2-C(carbyne) 1.875; carbyne-N 1.298; Fe1-Fe2 2.505; Fe1-C(CO) 1.780; Fe2-C(CO) 1.780; Fe1-C(μ-CO) 1.933; Fe2-C(μ-CO) 1.905; average Fe1-C(Cp) 2.119; average Fe2-C(Cp) 2.116; average Fe3-C(Cp) 2.056.

The geometric parameters extracted from the calculated DFT structures are in line with those observed in other diiron aminocarbyne complexes reported previously.[24,47] In particular, the carbyne-nitrogen bond distance (1.297 Å in the *cis* isomer) is indicative of a partial iminium character. Besides, the average Fe-carbyne distance (1.875 Å in the *cis* isomer) is considerably shorter than the average Fe-μ-CO distance (1.914 Å in the *cis* isomer). These data highlight the greater π-acceptor ability of the (ferrocenyl)aminocarbyne ligand compared to the CO ligand.[22,49] This leads the aminocarbyne to preferentially occupy a bridging coordination site over a terminal one, as such arrangement enhances the electron backdonation from the iron atoms.[22] The bonding situation in **[2]**$^+$ can be therefore described in terms of the resonance forms depicted in Scheme 2. In detail, the competition for the

vacant p-orbital on the carbyne carbon, between the nitrogen lone pair and the backdonation from the irons, results in a substantial charge delocalization.

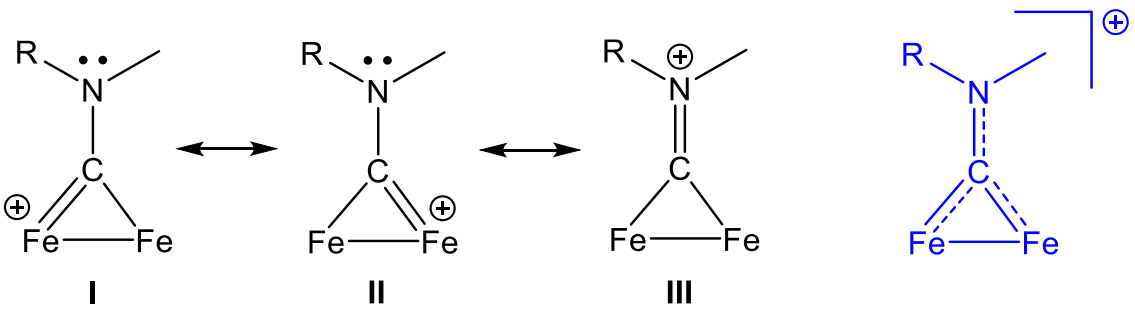

Scheme 2. Bonding of the bridging {CN(Me)R} ligand (including R = Fc as in **[2]**$^+$) to the {$Fe_2Cp_2(CO)_3$} fragment: **I**, **II**: aminocarbyne resonance structures; **III**: iminium resonance structure. In blue, comprehensive representation with a delocalized positive charge.

The experimentally detected *cis*/*trans* ratio (= 5 in $CDCl_3$ solution) is significantly lower than the theoretical value (11, in $CHCl_3$ as continuous medium). In general, the *cis*/*trans* isomerization for cationic tris-carbonyl μ-aminocarbyne complexes is not accessible at least up to 50 °C.[48,50] Therefore, to promote a potential isomerization process, solutions of **[2]CF_3SO_3** in various solvents were heated (Table 3). The greatest change in the *cis*/*trans* ratio was achieved by refluxing an acetone solution of **[2]CF_3SO_3** for 2.5 hours, resulting in an 18:1 *cis*/*trans* ratio. Consistently, DFT calculations considering acetone as an implicit solvent pointed out that ***cis*-[2]**$^+$ is more stable than ***trans*-[2]**$^+$ by approximately 1.7 kcal mol^{-1}, corresponding to a *cis*/*trans* ratio of 17 at 298 K. However, some degradation was observed in all tested conditions, leading to the formation of non carbonyl by-products which could not be identified. We presume that the isomerization process, if any, follows the Adams-Cotton mechanism via a terminal aminocarbyne species (see above).[22] In the NMR spectra of **[2]CF_3SO_3** (Figures S6-S8), each isomer displays nonequivalent Cp ligands within the {$Fe_2Cp_2(CO)_3$} core, due to the double bond character of the μ-C-N bond (vide infra), which hinders rotation around the C-N axis [e.g. for ***cis*-[2]**$^+$: δ(^{1}H) = 5.36, 4.84 ppm; δ(^{13}C) = 90.5, 90.4 ppm]. The Cp ring belonging to the ferrocenyl moiety exhibits lower chemical shift values [δ = 4.43 (^{1}H) and 70.5 ppm

(^{13}C) for ***cis*-[2]$^{+}$**]. The predominant *cis* isomer displays ^{13}C NMR resonances for the carbonyl ligands at 255.3 (bridging CO), 209.1 and 207.9 ppm (terminal CO). Accordingly, the IR spectrum of **[2]CF$_3$SO$_3$** (in CH_2Cl_2) contains three bands associated with the stretching vibrations of the terminal (2024 and 1992 cm^{-1}) and bridging carbonyl ligands (1837 cm^{-1}). Notably, the IR absorptions for the two isomers are almost identical, with the bands substantially overlapping (Figure S5).

Key spectroscopic features are those related to the {μ-CN} unit, manifesting in an infrared absorption at 1527 cm^{-1} and a ^{13}C NMR resonance at 326.8 ppm. Literature data concerning diiron aminocarbyne complexes of general formula $[Fe_2Cp_2(CO)_2(\mu\text{-}CO)\{\mu\text{-}CN(Me)(R)\}]^+$ range from 1522 (R = 2,6-C_6H_3MeCl) to 1604 cm^{-1} (R = Me) and 331.5 (R = 2,6-C_6H_3MeCl) to 315.5 ppm (R = Me), respectively, and clearly correlate with the electron donor properties of the R substituent.[22,24] The values obtained for **[2]CF$_3$SO$_3$** (R = Fc) approximate those of the analogous complex with R = 2,6-C_6H_3MeCl, outlining that the ferrocenyl moiety behaves electronically as an aryl within the cationic aminocarbyne moiety. We note that ferrocenyl has been previously regarded as an electron donor group in various systems; for instance, its donor capability has been estimated to exceed that of the methyl group in organophosphorus compounds,[51] and to approximate that of the 4-aminophenyl within W propargylidyne complexes.[52]

For sake of comparison, we synthesized the unprecedented *N*-phenyl aminocarbyne complex $[Fe_2Cp_2(CO)_2(\mu\text{-}CO)\{\mu\text{-}CN(Me)(Ph)\}]CF_3SO_3$, **[3]CF$_3SO_3$**, following the two-step method described for **[2]CF$_3$SO$_3$** (Scheme 1). Briefly, freshly prepared phenyl isocyanide (from phenyl formamide, see the Experimental section) was allowed to react with $[Fe_2Cp_2(CO)_4]$ in acetonitrile at room temperature. This reaction resulted in the formation of the known dark-violet compound $[Fe_2Cp_2(CO)_2(\mu\text{-}CO)(\mu\text{-}CNPh)]$,[53,54,55,56] which was isolated through alumina chromatography. Subsequent methylation with CF_3SO_3Me in CH_2Cl_2 followed by chromatographic purification afforded a red powder of the aminocarbyne complex **[3]CF$_3$SO$_3$**. The latter was isolated in *ca*. 41% yield, together with a minor amount of $[Fe_2Cp_2(CO)(CNPh)(\mu\text{-}CO)\{\mu\text{-}CN(Me)(Ph)\}]^+$ (unprecedented). The moderate yield and the

formation of by-products appears ascribable to the thermal instability and the enhanced reactivity of phenyl isocyanide promoted by metal coordination. The thermal or photolytic displacement of CO from $[Fe_2Cp_2(CO)_4]$ using PhNC was previously found to give $[Fe_2Cp_2(CO)_2(\mu\text{-}CO)(\mu\text{-}CNPh)]$ in 10−50 % yields, in admixture with the disubstituted derivative $[Fe_2Cp_2(CO)_2(CNPh)_2]$.[53,54] A similar reaction involving $[Ru_2Cp_2(CO)_4]$ resulted in the complete decomposition of the isocyanide.[45] Additionally, $[Fe_2Cp_2(CO)_2(\mu\text{-}CO)(\mu\text{-}CNPh)]$ was obtained in low to modest yields (5-46 %) from other monoiron or diiron precursors.[55-56]

The novel *N*-phenyl aminocarbyne complex **[3]CF_3SO_3** is air-stable and was characterized by IR and NMR spectroscopy (Figures S10-S14). The spectroscopic data for the {μ-CN} moiety well match the corresponding ones for **[2]CF_3SO_3** (IR absorption at 1527 and 1531 cm^{-1} and ^{13}C NMR resonance at 326.8 and 324.5 ppm, respectively in **[2]CF_3SO_3** and **[3]CF_3SO_3**).

The cation $\mathbf{[3]^+}$ was computationally optimized at C-PCM/PBEh-3c level, considering $CHCl_3$ as the solvent. Interestingly, the *cis* isomer exhibited higher stability than the *trans* isomer by about 3.7 kcal mol^{-1}. This outcome aligns with the experimental detection of a single species, ***cis*-$\mathbf{[3]^+}$**, in solution. The DFT-optimized structure of ***cis*-$\mathbf{[3]^+}$** is shown in Figure 3 and selected computed bond lengths are collected in the caption. Figure S15 shows a comparative view of the *cis* and *trans* isomers of $\mathbf{[3]^+}$.

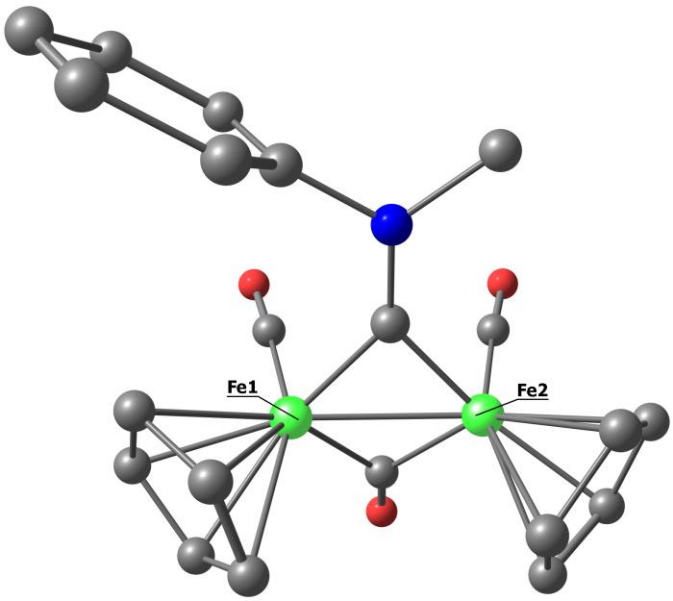

Figure 3. DFT optimized geometry of ***cis*-[3]$^+$**, computed at PBEh-3c level ($CHCl_3$ as continuous medium). Fe, green; N, blue; C, grey. Hydrogen atoms were omitted for clarity. Selected computed bond lengths: Fe1-C(carbyne) 1.859; Fe2-C(carbyne) 1.844; C(carbyne)-N 1.291; Fe1-Fe2 2.491; Fe1-C(CO) 1.774; Fe2-C(CO) 1.772; Fe1-C(μ-CO) 1.903; Fe2-C(μ-CO) 1.937; average Fe1-C(Cp) 2.105; average Fe2-C(Cp) 2.107.

In order to compare the electronic properties of the ferrocenyl- and phenyl-substituted aminocarbyne ligands, Extended Charge Decomposition Analyses (ECDA)[57] were carried out. A positive charge was assigned to the aminocarbyne moiety. The net electron transfer from $\{Fe_2Cp_2(CO)_2(\mu\text{-}CO)\}$ to $[CN(Me)Fc]^+$ is calculated to be 0.754, and a closely related value of 0.784 was determined for $[CN(Me)Ph]^+$. This similarity of values suggests that, overall, the two ligands exhibit comparable coordination features and electronic trends, in agreement with the key spectroscopic data discussed above. Furthermore, it is remarkable that the carbonyl regions of the simulated IR spectra of **[2]**$^+$ and **[3]**$^+$ are superimposable, as evident in Figure S16.

2. Electrochemical studies and DFT results

The redox chemistry and the *in situ* IR spectroelectrochemistry (IR SEC) of **[2]CF_3SO_3** and **[3]CF_3SO_3** were investigated in dichloromethane and THF solutions containing $[N^nBu_4]PF_6$ (0.2 mol dm^{-3}) as the supporting electrolyte. The aminocarbyne complexes **[4]CF_3SO_3** and **[5]CF_3SO_3** (Scheme 1) were

included in this study for comparative purposes. Table 1 collects the formal electrode potentials of the observed redox changes.

The presence of the ferrocenyl substituent within $[\mathbf{2}]^+$ becomes evident from the comparison of the cyclic voltammetries of $[\mathbf{2}]^+$ and $[\mathbf{3}]^+$ in the positive potential region. In CH_2Cl_2 solution, $[\mathbf{2}]^+$ displays one diffusion controlled, mono-electronic oxidation at +0.28 V *vs*. $FeCp_2$. This process exhibits features of chemical reversibility in the cyclic voltammetric time scale (Figure 4a) and can be attributed to the Fe^{II}-ferrocenyl moiety of the triiron complex. On the other hand, a two-electron, partially chemically reversible oxidation at a higher potential (about +0.97 V *vs*. $FeCp_2$) was observed in the CV profiles of $\mathbf{[3]}^+$ (Figure 4b), $\mathbf{[4]}^+$ and $\mathbf{[5]}^+$ (Table 1). This result seems consistent with a previous electrochemical study conducted on $\mathbf{[6]CF_3SO_3}$ and $\mathbf{[7]CF_3SO_3}$ in acetonitrile.[58]

When the oxidation process of $[\mathbf{2}]^+$ was investigated by *in situ* IR-SEC in an optically transparent thin-layer electrochemical (OTTLE) cell,[59] a blueshift of the IR absorption bands due to CO-stretching modes of terminal and bridging CO ligands of $[\mathbf{2}]^+$ (from 2024, 1992 and 1837 cm^{-1} to 2033, 2002 and 1845 cm^{-1}) was detected as the working electrode (WE) potential increased from +0.1 to +0.5 V (*vs*. $FeCp_2$), Figure 5. This shift corresponds to the quantitative formation of the one-electron oxidation product $[\mathbf{2}]^{2+}$. The latter remained stable within the time scale of the spectroelectrochemical experiment, indeed the initial spectrum was almost completely restored during the reverse reduction scan.

The slight shift (approximately +10 cm^{-1}) of the wavenumbers agrees with the assumption that the reversible one-electron removal primarily affects the ferrocenyl portion of the complex, thereby having minimal impact on the carbonyl ligands bound to the Fe_2Cp_2 core.

In the negative potential range, all the complexes $[\mathbf{2}]^+$–$[\mathbf{5}]^+$ undergo a monoelectronic, diffusion controlled, and electrochemically reversible reduction at approximately the same potential. However, this reduction is complicated by subsequent chemical reactions (with i_b/i_f ratios of 0.84 and 0.83 at a scan rate of 100 $mV \cdot s^{-1}$ for $[\mathbf{2}]^+$ and $[\mathbf{3}]^+$, respectively).

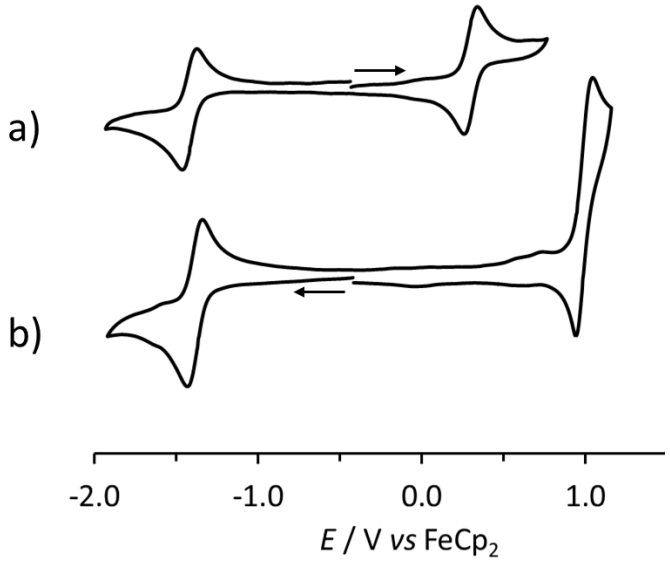

Figure 4. CV recorded at a Pt electrode in a CH_2Cl_2 solution of a) [**2**]$^+$ between −1.92 and +1.16 V; b) [**3**]$^+$ between −1.92 and +1.58 V. [^{n}Bu$_4$N]PF_6 (0.2 mol dm^{-3}) as supporting electrolyte. Scan rate: 0.1 V·s^{-1}. The arrows indicate the direction of the scan.

Table 1. Formal electrode potentials (V, *vs*. $FeCp_2$ and, in brackets, *vs*. Ag/AgCl) and peak-to-peak separations (mV) for the redox processes exhibited in CH_2Cl_2 or THF solutions and aqueous media by [**2**]$^+$, [**3**]$^+$**,** [**4**]$^+$ and [**5**]$^+$.

Compound	Oxidation processes				Reduction process	
	$E°_1$	ΔE_p[a]	$E°_2$	ΔE_p[a]	$E°_3$	ΔE_p[a]
[**2**]CF_3SO_3[b]	+1.28[e] (+1.73)		+0.28 (+0.73)	80	–1.44 (–0.99)	83
[**3**]CF_3SO_3[b]	+0.97 (+1.42)	101			–1.41 (–0.96)	88
[**4**]CF_3SO_3[b]	+0.97 (+1.42)	95			–1.40 (–0.95)	84
[**5**]CF_3SO_3[b]	+0.95 (+1.40)	120			–1.41 (–0.96)	84
[**2**]CF_3SO_3[c]	+0.24 (+0.81)	85			–1.42 (–0.85)	85
[**3**]CF_3SO_3[c]	+1.03[e] (+1.60)				–1.40 (–0.83)	80
[**4**]CF_3SO_3[c]	+1.05[e] (+1.62)				–1.42 (–0.85)	80
[**4**]CF_3SO_3[d]	+0.90[e] (+1.10)				–1.17 (–0.97)	96

[**5**]CF_3SO_3[d]	+0.90[e] (+1.10)				–1.18 (–0.98)	96

[a]Measured at 0.1 V/s. [b]In CH_2Cl_2/[^{n}Bu$_4$N]PF_6. [c]In THF/[^{n}Bu$_4$N]PF_6. [d]In phosphate buffer. [e]Peak potential value for irreversible processes.

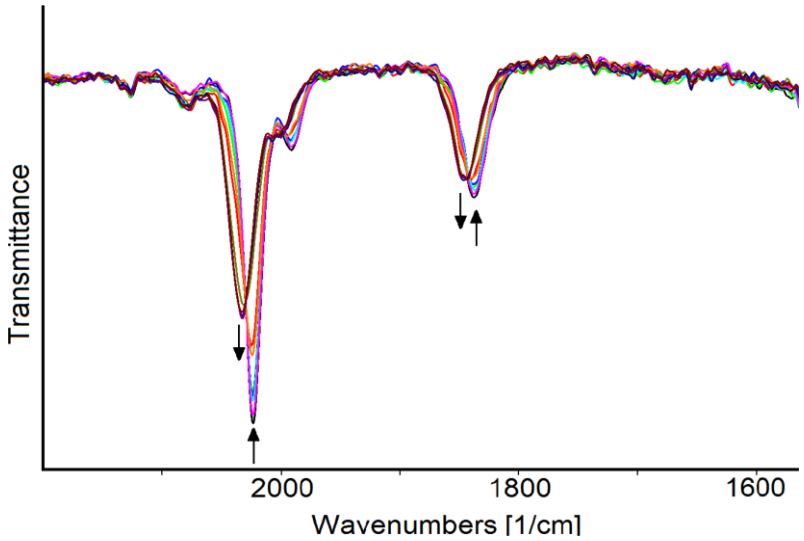

Figure 5. IR spectra of a CH_2Cl_2 solution of **[2]CF_3SO_3** recorded in an OTTLE cell during the progressive increase of the WE potential from +0.1 to +0.5 V (*vs* $FeCp_2$; scan rate 1 mV·sec^{-1}). [^{n}Bu$_4$N]PF_6 (0.2 mol dm^{-3}) as the supporting electrolyte. The absorptions of the solvent and supporting electrolyte have been subtracted.

Collectively, the *in-situ* IR spectroelectrochemical (IR SEC) analyses of [**2**]$^+$–[**5**]$^+$ in CH_2Cl_2/[^{n}Bu$_4$N]PF_6 solutions indicate that electron addition mainly involves the [Fe^IFe^I] core.

As the potential of the working electrode gradually decreased from −1.3 to −1.6 V (*vs*. $FeCp_2$), the IR absorptions of [**2**]$^+$ were initially replaced by new bands at lower wavenumbers (ν_{CO} = 1958, 1919 and 1741 cm^{-1}, Figure S17a), attributed to the neutral radical species [**2**]$^\bullet$. However, prior to the complete disappearance of [**2**]$^+$, a slight blueshift of the IR absorption bands due to the stretching modes of terminal and bridging CO ligands of the newly formed [**2**]$^\bullet$ was detected (ν_{CO} = 1963, 1928 and 1773 cm^{-1}, Figure S17b). This process was completed within the following 10 minutes during microelectrolysis at a constant potential of −1.8 V (Figure S17c). Instead, the spectral changes recorded in the OTTLE cell over 10 minutes after the complete reduction of [**2**]$^+$, without an applied potential, suggest that a disproportionation reaction of [**2**]$^\bullet$ occurs subsequent to the electron transfer. This

reaction results in the regeneration of $[\mathbf{2}]^+$ and the formation of an unidentified species, **2*** (ν_{CO} = 1963, 1928 and 1773 cm^{-1}, Figure S18). Evidence of a disproportionation reaction of $[\mathbf{2}]^{\bullet}$ and the bulk electrolysis to determine the electron stoichiometry of the transformation $[\mathbf{2}]^+ \rightarrow$ **2*** (Figure S19) are supplied in the SI.

The formation of the tris-carbonyl complex **2*** (ν_{CO} = 1963, 1928 and 1773 cm^{-1}) is restricted to the use of dichloromethane as solvent, and we hypothesize that it is consequent to the generation of radical species (X) from CH_2Cl_2, converting the bridging aminocarbyne ligand, CN(Me)(Fc), into a bridging aminocarbene, C(X)N(Me)(Fc).[47] We verified that in THF/$[^nBu_4N]PF_6$ solutions the reduction of $[\mathbf{2}]^+$ is fully reversible (i_b/i_f = 1 at a scan rate of 100 $mV \cdot s^{-1}$) (Table 1) and, consistently, an IR SEC experiment confirmed that the reduction of $[\mathbf{2}]^+$ (ν_{CO} = 2016, 1986 and 1834 cm^{-1}) leads to the quantitative and entirely reversible formation of $[\mathbf{2}]^{\bullet}$ (ν_{CO} = 1956, 1919 and 1757 cm^{-1}), also in the long time scale of this experiment (Figure 6).

A parallel behavior was observed for $[\mathbf{3}]^+$–$[\mathbf{5}]^+$, in both CH_2Cl_2 and THF (Figure S20 refers to $[\mathbf{3}]^+$ as a representative compound), confirming that the reactivity of the radicals $[\mathbf{2}]^{\bullet}$–$[\mathbf{5}]^{\bullet}$ in dichloromethane is a general trend, which is related to the intervention of the solvent and independent of the presence of the ferrocenyl moiety.[60] The large redshift of the IR absorption bands due to stretching modes of terminal and bridging CO ligands upon reduction (about 70 cm^{-1} for both complexes) suggests that the LUMO is mainly localized on the $Cp_2Fe^I_2$ core, in agreement with previous DFT outcomes on the *N*-dimethyl derivative $[\mathbf{6}]^+$ (Scheme 1).[61]

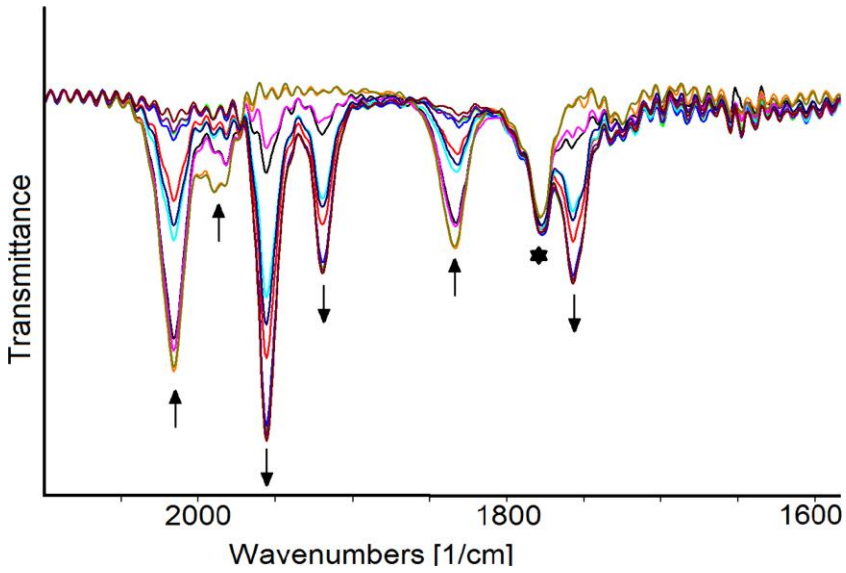

Figure 6. IR spectra of a THF solution of [**2**]$^{+}$ recorded in an OTTLE cell during the progressive decrease of the WE potential from –1.2 to –1.6 V (*vs* $FeCp_2$; scan rate 1 mV sec^{-1}) Starred peak is due to impurities. [$^{n}Bu_4N]PF_6$ (0.2 mol dm^{-3}) as the supporting electrolyte. The absorptions of the solvent and supporting electrolyte have been subtracted.

The structures of both the *cis* and *trans* isomers of the radical **[2]**$^{\bullet}$ were computationally optimized and are shown in Figure 7. The ***cis*-[2]**$^{\bullet}$ isomer resulted more stable than ***trans*-[2]**$^{\bullet}$ by approximately 1.8 kcal·mol^{-1}, considering acetone as the continuous medium. The optimized structures closely resemble those of the parent cations, exhibiting root mean square deviation (RMDS) values ranging from 0.118 to 0.133Å. This outcome is in line with the electrochemical reversibility described above. The simulated IR spectra of ***cis*-[2]**$^{\bullet}$ and ***trans*-[2]**$^{\bullet}$, compared to the corresponding parent cationic complexes, highlight the significant shift of the carbonyl stretching vibrations towards lower wavenumbers (Figure S22). The spin density plots depicted in Figure 7 confirm that the reduction process involves the {Fe(μ-CO)Fe} fragment, while the contribution of the ferrocenyl unit appears negligible.

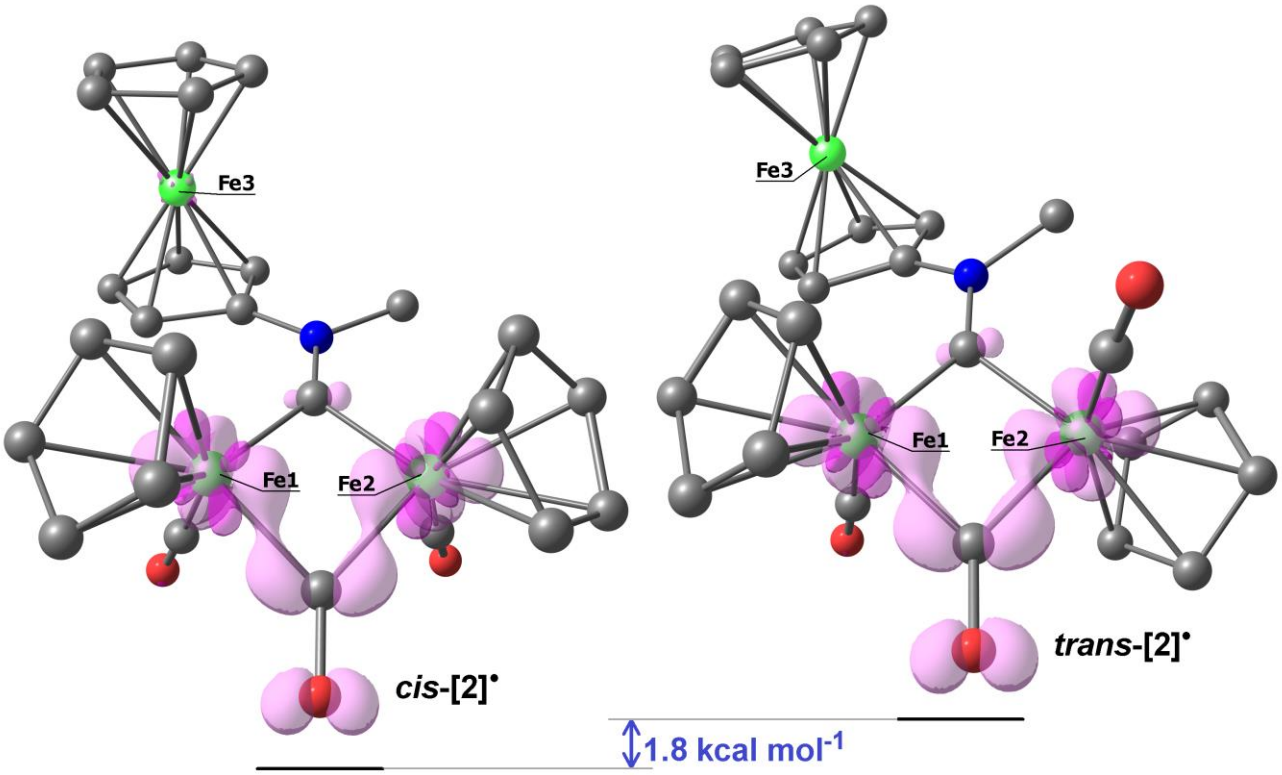

Figure 7. DFT optimized geometries of ***cis*-[2]•** (left) and ***trans*-[2]•** (right), computed at PBEh-3c level (acetone as continuous medium). Fe, green; N, blue; C, grey. Hydrogen atoms were omitted for clarity. Spin density surfaces (isovalue = 0.01 a.u.) in pink tones. Selected computed bond lengths for ***cis*-[2]•** (Å): Fe1-C(carbyne) 1.886; Fe2-C(carbyne) 1.917; C-N 1.310; Fe1-Fe2 2.678; Fe1-C(CO) 1.743; Fe2-C(CO) 1.745; Fe1-C(μ-CO) 1.931; Fe2-C(μ-CO) 1.916; average Fe1-C(Cp) 2.176; average Fe2-C(Cp) 2.158; average Fe3-C(Cp) 2.058. Selected computed bond lengths for ***trans*-[2]•** (Å): Fe1-C(carbyne) 1.873; Fe2-C(carbyne) 1.899; C-N 1.311; Fe1-Fe2 2.714; Fe1-C(CO) 1.748; Fe2-C(CO) 1.752; Fe1-C(μ-CO) 1.930; Fe2-C(μ-CO) 1.930; average Fe1-C(Cp) 2.178; average Fe2-C(Cp) 2.158; average Fe3-C(Cp) 2.057.

In summary, within the triiron species [**2**]$^+$, the two iron-based redox systems (i.e., the ferrocenyl Fe^{II} and $Fe^{I}Fe^{I}$) are independent.

The redox properties of **[4]CF_3SO_3** and **[5]CF_3SO_3** were additionally investigated in a phosphate buffer (PB; pH = 7.3), given the sufficient solubility of these complexes in aqueous media. In the PB, the oxidation process for both [**4**]$^+$ (Figure S21) and [**5**]$^+$ is irreversible, multielectronic, and shifted at lower potentials by approximately 300 mV compared to the organic solvent.[62] Conversely, a reduction occurs at potential values similar to those recognized in CH_2Cl_2 solution. In the backscan, we observed an absorption peak probably due to the neutral complexes **4•** and **5•**.

Anyway, both the reduction and oxidation potentials of [**4**]$^+$ and [**5**]$^+$ fall outside the biologically relevant potential range, which approximately covers the window –0.4 to +0.8 V *vs*. SHE (–0.6 to +0.6 V *vs*. Ag/AgCl).[63,64] The limited water solubility of **[2]CF$_3$SO$_3$** prevented its CV characterization in the PB solution. Nevertheless, if we assume that the behavior difference of **[2]**$^+$ when varying the solvent parallels that of **[4]**$^+$ and **[5]**$^+$, the potential for achieving biooxidative activation could be accessible for the *N*-ferrocenyl aminocarbyne complex.

3. Behavior of diiron complexes in aqueous media and biological studies

In preparation for the biological investigation, we conducted an initial assessment of **[2]CF$_3$SO$_3$** and **[3]CF$_3$SO$_3$** in aqueous solutions. By using established ^{1}H NMR and UV-Vis methods, we assessed the water (D_2O) solubility, the octanol-water partition coefficient and the stability of the complexes under conditions relevant to biology (37 °C, cell culture medium), see Table 2. The change from a phenyl to a ferrocenyl group in the aminocarbyne ligand is accompanied by decreased water solubility and increased lipophilicity. Nevertheless, both **[2]CF$_3$SO$_3$** and **[3]CF$_3$SO$_3$** can be categorized as *amphiphilic* compounds ($-0.5 < \text{Log } P_{ow} < +0.5$). These compounds exhibited substantial stability at 37 °C, with 62-74 % of the starting material remaining unchanged after 48 h in D_2O solution or after 24 h in DMEM cell culture medium.[65]

Interestingly, ^{1}H NMR spectroscopy showed for the aqueous solutions of **[2]**$^+$ an enrichment in the *trans* isomer (*cis*/*trans* ratio ≈ 1), deviating from the situation observed in $CDCl_3$ (see above). We did not collect evidence of an oxidation of the ferrocenyl unit in [**2**]$^+$ in such aerobic environments (E° = + 0.83 V *vs* SHE for O_2/H_2O at pH = 7).

Table 2. Behavior of diiron aminocarbyne complexes in aqueous solutions (see Experimental for details). Solubility in D_2O (^{1}H NMR, Me_2SO_2 internal standard) and octanol/water partition coefficient (Log P_{ow}; UV-Vis) at 21±1 °C. Relative stability in D_2O/CD_3OD and DMEM-d/CD_3OD mixtures (5:2 v/v) at 37 °C after 48 or 24 h, respectively (^{1}H NMR, Me_2SO_2 internal standard).

	[2]CF$_3$SO$_3$	**[3]CF$_3$SO$_3$**

Solubility / mol·L^{-1}	< $3 \cdot 10^{-4}$ [a]	$1.6 \cdot 10^{-3}$
Log P_{ow}	0.55 ± 0.05	− 0.38 ± 0.02
Residual complex % in D_2O/CD_3OD	62 %	68 %
Residual complex % in DMEM-d/CD_3OD	65 %	74 %

[a] Below the lowest value of quantitation.

Several diiron aminocarbyne complexes were previously investigated for their in vitro anticancer activity (see Introduction), that is strongly influenced by the nature of the aminocarbyne substituents (Figure 1, structure **I**). For instance, while **[6]CF_3SO_3** does not exhibit cytotoxicity, **[4]CF_3SO_3** and **[5]CF_3SO_3** have showcased a significant antiproliferative activity against various human cancer cell lines.[23,24] Their mechanism of action has been mainly associated with their capacity to interfere with cellular redox processes through the intracellular release of iron(I) species.[24] The incorporation of the ferrocenyl in **[2]CF_3SO_3** introduces an additional redox-active fragment that could potentially participate in intracellular biological processes (see Introduction). On the other hand, **[3]CF_3SO_3**, lacking the ferrocenyl unit, serves as a benchmark for comparison,[66] especially when considering the similar electronic properties revealed by the bridging ligands CNMe(Fc) (in **[2]**$^+$) and CNMe(Ph) (in **[3]**$^+$), vide infra.

The cytotoxicity of **[2]CF_3SO_3** and **[3]CF_3SO_3** was evaluated across a range of human cancer cell lines representative of different solid tumors. In particular, the in-house cancer cell panel includes examples of human cervical (A431), colon (HCT-15), pancreatic (PSN-1), and ovarian (2008) carcinoma as well as of small-cell lung cancer (SCLC, U1285). The cytotoxicity parameters, expressed in terms of IC_{50} values acquired following 72 hours of exposure to the MTT assay, are reported in Table 3. For comparison purposes, the cytotoxicity of the reference metal-based chemotherapeutic drug cisplatin was assessed under the same experimental conditions.

Table 3. Cytotoxic activity of diiron complexes and cisplatin in 2D models.

	IC_{50} (μM) ± S.D.				
	A431	**HCT-15**	**PSN-1**	**2008**	**U1285**
[2]CF_3SO_3	60 ± 14	33 ± 12	23.1 ± 4.6	32.9 ± 2.8	16.0 ± 1.3
[3]CF_3SO_3	75.1 ± 8.9	86.2 ± 0.5	> 100	86 ± 11	50.8 ± 6.7
Cisplatin	1.7 ± 0.3	13.9 ± 1.6	12.1 ± 2.8	2.1 ± 1.1	6.9 ± 1.1

Cells (3-8 x 10^3 cell/well) were treated for 72 hours with increasing concentrations of tested compounds. Cytotoxicity was assessed by MTT test. The IC_{50} values were calculated by the four-parameter logistic model ($p < 0.05$). S.D. is standard deviation.

Both **[2]CF_3SO_3** and **[3]CF_3SO_3** showed a moderate cytotoxicity profile, with average IC_{50} values generally higher compared to cisplatin over the five tested human cancer cell lines. Within the diiron complexes, the ferrocenyl derivative **[2]CF_3SO_3** is significantly more effective than the *N*-phenyl analogue **[3]CF_3SO_3**. On average, the *in vitro* antitumor activity of **[2]CF_3SO_3** exceeded that of **[3]CF_3SO_3** by a factor of 2.4. In particular, **[2]CF_3SO_3** outperformed **[3]CF_3SO_3** against pancreatic adenocarcinoma (PSN-1) and SCLC cells, showing 4-fold and 3-fold higher efficacy, respectively.

Although 2D cell cultures are widely employed for *in vitro* screening due to their low cost, simplicity and reliability, they are unable to mimic the properties of *in vivo* solid tumors. In contrast, 3D cell cultures offer greater efficiency in reproducing the heterogeneity and complexity of tumor masses, and therefore they are more predictive of *in vivo* outcomes than traditional 2D cell cultures.[67] On these bases, the cytotoxicity of **[2]CF_3SO_3** and **[3]CF_3SO_3** was also examined using a 3D cell culture model of SCLC cells. Hence, U1285 cells were treated with the investigated compounds for 72 hours, and cell viability was assessed by means of the acid phosphatase (APH) assay (Table 4).

Table 4. Cytotoxicity (IC_{50} values, μM) of diiron complexes and cisplatin in a SCLC 3D model.

	U1285
[2]CF_3SO_3	51.3 ± 4.2

[3]CF_3SO_3	>100
Cisplatin	65.4 ± 1.4

Spheroids (2.5 x 10^3 cells/well) were treated for 72 hours with increasing concentrations of tested compounds. The growth-inhibitory effect was evaluated by means of the acid phosphatase (APH) test. IC_{50} values were calculated from the dose–survival curves using a four-parameter logistic model ($p < 0.05$). S.D. = standard deviation.

Remarkably, the 3D cytotoxicity studies not only confirmed the superior anticancer potential of the ferrocenyl derivative **[2]CF_3SO_3** with respect to the phenyl-analogue **[3]CF_3SO_3**, but also unveiled the higher activity of **[2]CF_3SO_3** than the reference drug cisplatin, within a tridimensional environment.

Afterwards, we evaluated the ability of **[2]CF_3SO_3** and **[3]CF_3SO_3** to increase the total basal production of reactive oxygen species (ROS) in U1285 cancer cells. As clearly shown in Figure 8, **[2]CF_3SO_3** triggered a substantial time-dependent rise in the cellular basal hydrogen peroxide production, similar to the effect induced by antimycin, a well-known inhibitor of mitochondrial Complex III in the respiratory chain. Complex **[3]CF_3SO_3** was also effective in enhancing cellular basal ROS production, although to a significantly lower extent. Overall, collected data and previous findings on related diiron complexes suggest that the here described triiron complexes exert their antitumoral effect inside the cells, and specifically mitochondria represent a probable, preferential target.[23-27]

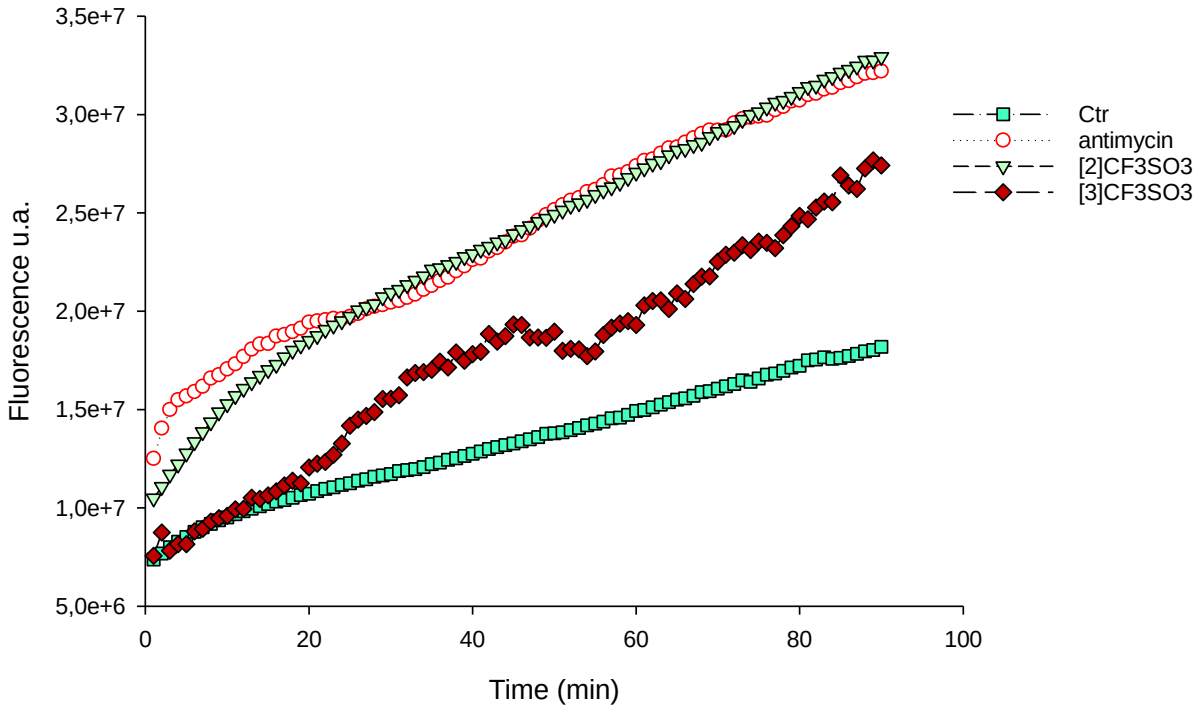

Figure 8. ROS production in U1285 cells. Cells were pre-incubated in PBS/10 mM glucose medium for 20 min at 37° C in the presence of 10 μM CM–H_2DCFDA and then treated with the tested compounds.

Concluding remarks

The ferrocene skeleton possesses distinct properties which have inspired its conjugation with other metal structures, pointing to various applications. Here, we have described the use of isocyanoferrocene as a ligand for the $Fe_2Cp_2(CO)_3$ scaffold, and its subsequent methylation to generate the first ferrocenyl-decorated aminocarbyne, **[2]**$^+$. Notably, the ferrocenyl substituent provides a stabilizing effect to the aminocarbyne system and the entire cationic complex, which is indefinitely air stable and exhibits a significant robustness in aqueous solutions under pseudo-physiological conditions. Spectroscopic data and DFT outcomes highlight that the *N*-ferrocenyl aminocarbyne ligand behaves as a moderate π-acceptor strictly similar to its *N*-phenyl counterpart. In comparison to related diiron complexes, the triiron complex **[2]**$^+$ exhibits a distinct electrochemical behavior, consisting in reduction and oxidation events centered at the [Fe^IFe^I] core and the Fe^{II} of the ferrocenyl, respectively. Cellular

experiments conducted on both the *N*-ferrocenyl, **[2]**$^+$, and *N*-phenyl, **[3]**$^+$, aminocarbyne complexes suggest that the unique combination of electrochemical properties in **[2]**$^+$ is key to its enhanced ability to trigger the production of reactive oxygen species within cancer cells. It is remarkable that, while **[2]**$^+$ displays an averagely moderate 2D antiproliferative activity against cancer cell lines, its performance in a more reliable 3D model exceeds that of the clinical drug cisplatin. The conjugation of an easily available diiron framework with the ferrocenyl moiety represents a promising strategy with potential implications in drug development.[28] Future studies will focus on the modification of **[2]**$^+$ exploiting the arsenal of reactions documented for analogous diiron aminocarbyne complexes,[19] aiming to produce novel organometallic structures with, hopefully, optimized characteristics and pharmacological profiles.

Experimental.

1. General experimental details.

Reactants and solvents were purchased from Alfa Aesar, Merck, Strem or TCI Chemicals, and were of the highest purity available. $POCl_3$ and Et_3N (over 4 Å MS) were stored under N_2 atmosphere as received. Syntheses were conducted under N_2 atmosphere using standard Schlenk techniques and products were conserved under N_2 once isolated. Complexes **[4,5]CF_3SO_3** were prepared according to the literature.[24] Dichloromethane, tetrahydrofuran, and diethyl ether were dried with the solvent purification system mBraun MB SPS5, while acetonitrile was distilled from CaH_2 and diisopropylamine from BaO. Chromatography separations were carried out on columns of silica gel (70–230 mesh), neutral alumina or deactivated alumina (Merck, 4% *w/w* water) using solvents from the bottle under N_2 flux. IR spectra of solutions were recorded using a CaF_2 liquid transmission cell (1500-2300 cm^{-1}) on a Perkin Elmer Spectrum 100 FT-IR spectrometer. IR bands attributed to terminal and bridging CO/CNR ligands are indicated as t-CO/t-CN and μ-CO/μ-CN, respectively. UV-vis spectra were recorded on an Ultraspec 2100 Pro spectrophotometer using PMMA cuvettes (1 cm pathlength).

IR and UV-vis spectra were processed with Spectragryph.[68] NMR spectra were recorded on a Bruker Avance II DRX400 instrument equipped with a BBFO broadband probe. Chemical shifts are referenced to the residual solvent peaks[69] or external standard ($CFCl_3$ for ^{19}F NMR). NMR spectra were assigned with the assistance of ^{1}H NOESY, ^{1}H-^{1}H COSY and ^{1}H-^{13}C (*gs*-HSQC and *gs*-HMBC) correlation experiments.[70] NMR signals due to secondary isomeric forms (where it has been possible to detect them) are italicized. Elemental analyses were performed on a Vario MICRO cube instrument (Elementar).

2. Optimized synthesis and characterization of isocyanoferrocene and phenyl isocyanide

2.1. Isocyanoferrocene, CNFc (Scheme 3).

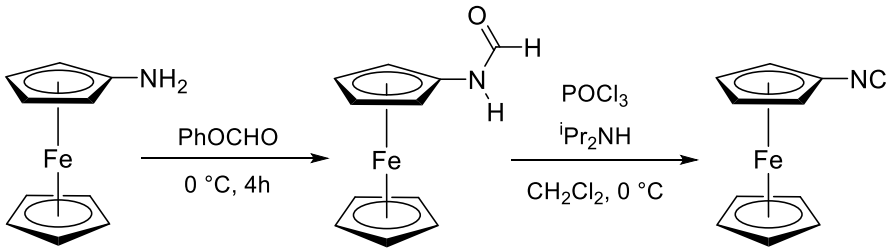

Scheme 3. Two-step synthesis of isocyanoferrocene.

This synthesis was performed with slight modifications to previously reported procedures.[38,71,72] Aminoferrocene was prepared using the procedure described in the SI (Scheme S1). In a Schlenk tube at 0 °C, phenyl formate (0.76 mL, 7.03 mmol) was added to aminoferrocene (707 mg, 3.51 mmol) and this mixture was stirred for 4 hours. Complete consumption of aminoferrocene was checked by TLC (eluent: Et_2O). All volatiles were removed under vacuum at 40 °C. The resulting brown oil was dissolved into a hexane/Et_2O mixture, and this solution was passed through a SiO_2 column. Elution with hexane allowed to remove impurities, then a bright-orange solution was collected using Et_2O as eluent. Drying under vacuum afforded an orange solid corresponding to ferrocenyl formamide (FcNHCHO). The solid was dissolved in CH_2Cl_2 (18 mL), then $POCl_3$ (0.33 mL, 3.51 mmol) and anhydrous diisopropylamine (2.48 mL, 17.6 mmol) were added. The resulting solution was stirred at 0

°C, and a color change from orange to brown was noticed along 2 hours. After stirring for 6 hours, the reaction mixture was quenched with 40 mL of 10 % aqueous K_2CO_3. The organic layer was separated and washed twice with 30 mL 10 % aqueous K_2CO_3 in air. Volatiles were removed under vacuum. The residue was dissolved in Et_2O/hexane (1:1 v/v) and this solution was passed through a SiO_2 column. Removal of volatiles under vacuum gave the title product as a crystalline orange solid. Yield 685 mg, 92 %. Anal. Calcd. for $C_{11}H_9FeN$: C, 62.60; H, 4.30; N, 6.64. Found: C, 62.38; H, 4.28; N, 6.84. IR (CH_2Cl_2): $\tilde{\nu}$/cm^{-1} = 2149w-sh, 2127s (C≡N). ^{1}H NMR ($CDCl_3$): δ/ppm = 4.55 (t, $^3J_{HH}$ = 2.0 Hz, 2H, C_5H_4); 4.30 (s, 5H, Cp); 4.12 (t, $^3J_{HH}$ = 2.0 Hz, 2H, C_5H_4).

2.2. Phenyl isocyanide, CNPh (Scheme 4).

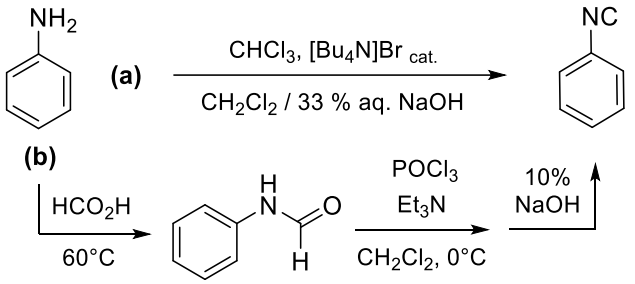

Scheme 4. Preparation of phenyl isocyanide from aniline according to the Hoffman (**a**) or Ugi (**b**) methodologies.

Hoffman method.[73,74,75] A solution of [Bu_4N]Br (50 mg, 0.15 mmol), aniline (490 mg, 5.3 mmol) and $CHCl_3$ (0.5 mL, 6 mmol) in CH_2Cl_2 (5 mL) was added under vigorous stirring to a 100 mL tube containing 33 % *wt*. aqueous NaOH (2.5 g / 5 mL). The biphasic mixture was stirred at ambient T overnight. Conversion was checked by IR, then the mixture was diluted with CH_2Cl_2, water and transferred into a separatory funnel. The aqueous phase was discarded; the organic phase was extracted with saturated $NaHCO_3$ (x2) and water. Volatiles were removed under vacuum without external heating (*Caution! PhNC is toxic, this operation must be performed in a well-ventilated fume hood*), affording an orange-brown oil (yield: 434 mg) that was immediately allowed to react with [$Fe_2Cp_2(CO)_4$]. Phenyl

isocyanide is highly sensitive to these reaction conditions, resulting in a non-reproducible yield and purity. Silica and/or alumina chromatography resulted in its complete degradation.

Ugi method. Phenyl formamide (250 mg, 2.06 mmol), prepared according to an optimized literature method[76] (see ESI), was dissolved in CH_2Cl_2 (6 mL) and treated with Et_3N (0.60 mL, 4.3 mmol). The pale-yellow solution was cooled to 0 °C then $POCl_3$ (0.20 mL, 2.1 mmol) was added dropwise. The mixture was stirred at 0 °C for 1 h then allowed to heat to ambient temperature and treated with 10 % NaOH (10 mL). The mixture was stirred for 10 minutes then diluted with H_2O and moved into a separatory funnel. The aqueous phase was extracted with CH_2Cl_2 (4 x 10 mL). The combined organic fractions were taken to dryness under vacuum without external heating (*Caution! PhNC is toxic, this operation must be performed in a well-ventilated fume hood*), affording a pale red oil that was immediately allowed to react with $[Fe_2Cp_2(CO)_4]$. IR (CH_2Cl_2): $\tilde{\upsilon}/cm^{-1}$ = 2130s (CN), 1648m-sh, 1626m, 1589m. IR (MeCN): $\tilde{\upsilon}/cm^{-1}$ = 2130s (CN), 1649m-sh, 1628m, 1589m. It is essential to perform the reaction below room temperature and to quench the final mixture with NaOH; workups in less basic condition (*e.g.* saturated $NaHCO_3$, 10 % Na_2CO_3) [77,78,79] resulted in extensive decomposition of the isocyanide.

3. Synthesis and characterization of diiron complexes

3.1. $[Fe_2Cp_2(CO)_2(\mu\text{-}CO)\{\mu\text{-}CN(Me)(Fc)\}]CF_3SO_3$, **[2]**$CF_3SO_3$ (Figure 9)

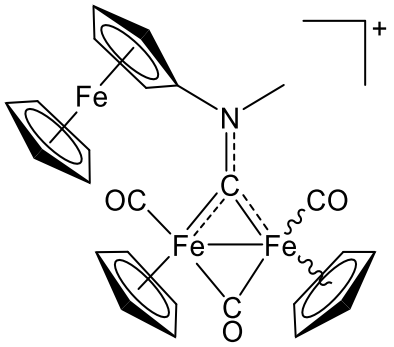

Figure 9. Structure of **[2]**$^+$.

A solution of $[Fe_2Cp_2(CO)_4]$ (430 mg, 1.21 mmol) in acetonitrile (15 mL) was treated with 1 equivalent of freshly synthesized isocyanoferrocene. The resulting dark-brown solution was stirred at room temperature. After 2 hours, a brown precipitate was formed, stirring was prolonged for further 20 hours, then volatiles were removed under reduced pressure. The resulting dark-brown solid contains $[Fe_2Cp_2(CO)_3(CNFc)]$, **1**, and a minor amount of unreacted $[Fe_2Cp_2(CO)_4]$. IR (CH_2Cl_2): $\tilde{\nu}/cm^{-1}$ = 2100w (t-CN), 1988s (t-CO), 1951s (t-CO), 1788m (μ-CO), 1751 (μ-CO), 1691s (μ-CN). IR (CH_3CN): $\tilde{\nu}/cm^{-1}$ = 2098w (t-CN), 1984s (t-CO), 1946s (t-CO), 1790m (μ-CO), 1753 (μ-CO), 1693s (μ-CN).

The residue was dissolved in CH_2Cl_2 (15 mL) and methyl triflate (0.13 mL, 1.2 mmol) was added dropwise to the stirred solution. The mixture was stirred at room temperature for 4 hours, then it was directly charged on top of a deactivated alumina column (length 6 cm, diameter 3.5 cm). Impurities were removed by using CH_2Cl_2 and CH_2Cl_2/THF (1:1 *v*/*v*) as eluents. A bright-red band corresponding to **[2]CF$_3$SO$_3$** was collected by using neat CH_3CN as eluent. According to ^{1}H NMR analyses, the eluted mixture was progressively enriched with the *cis* isomer and the final portion of the band contained pure *cis*-**[2]CF$_3$SO$_3$**. Solvent removal under reduced pressure allowed to obtain a red solid, which was washed with Et_2O and dried under vacuum. Yield 744 mg, 88 %. Soluble in DMSO, EtOH, CH_2Cl_2, acetone, insoluble in Et_2O. X-Ray quality crystals of **[2]CF$_3$SO$_3$** were obtained CH_2Cl_2/pentane at − 20°C. Anal. Calcd. for $C_{26}H_{22}F_3Fe_3NO_6S$: C, 44.54; H, 3.16; N, 2.00; S, 4.57. Found: C, 44.38; H, 3.21; N, 1.96; S, 4.62. IR (CH_2Cl_2): $\tilde{\nu}/cm^{-1}$ = 2024 (s, CO); 1992 (w-m, CO); 1837 (m, μ-CO); 1527 (w-m, μ-CN). ^{1}H NMR ($CDCl_3$, *cis*/*trans* ratio = 5): δ/ppm = 5.43, *4.71, 4.64,* 4.49, 4.41, 4.32, *4.20* (m, 4H, C_5H_4); 5.36, *5.23*, 4.84, *4.64* (s, 10H, Cp); 4.92, *4.89* (s, 3H, Me); *4.56*, 4.43 (s, 5H, Cp^{Fc}). ^{13}C{^{1}H} NMR ($CDCl_3$): δ/ppm = 326.8 (μ-CN); 255.3 (μ-CO); 209.1, 207.9 (CO); 121.0 (d, $^1J_{CF}$ = 321 Hz, CF_3); 112.1 (NC^{Cp}); *91.7*, 90.53, 90.48 (Cp); *70.8*, 70.5 (Cp^{Fc}); *67.7*, 67.5, *66.3*, 65.6, 65.4, 65.2 (C_5H_4); 60.5, *59.0* (Me). ^{19}F{^{1}H} NMR ($CDCl_3$): δ/ppm = - 78.1.

3.2. [Fe$_2$Cp$_2$(CO)$_2$(μ-CO){μ-CN(Me)(Ph)}]CF$_3$SO$_3$, [3]CF$_3$SO$_3$ (Figure 10).

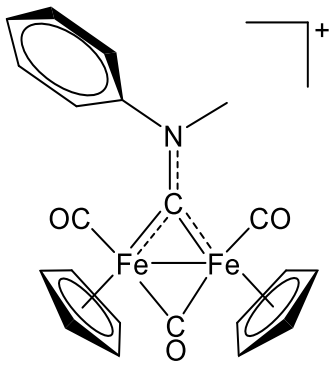

Figure 10. Structure of **[3]**$^{+}$.

In a 100 mL round bottom flask under N_2, freshly prepared PhNC (*ca*. 2 mmol) was dissolved in anhydrous MeCN (20 mL) and treated with $[Fe_2Cp_2(CO)_4]$ (730 mg, 2.06 mmol). The dark red suspension was stirred at room temperature overnight; a dark violet shade appeared in less than 1 h. Conversion was checked by IR (MeCN) then volatiles were removed under vacuum. The dark violet residue was suspended in Et_2O and treated with 48 % aq. HBF_4 (0.3 mL, 2.3 mmol), affording a scarlet red solid. The suspension was stirred for 2 h then moved on top of an alumina column (h 5 d 3.4 cm). A dark red band containing $[Fe_2Cp_2(CO)_4]$ and other impurities was eluted as using Et_2O, then a dark violet band was eluted using a 5 % Et_3N solution in CH_2Cl_2 (*ca*. 200 mL). Volatiles were removed under vacuum, affording a dark violet residue containing $[Fe_2Cp_2(CO)_2(\mu\text{-}CO)(\mu\text{-}CNPh)]$[80] {IR ($CH_2Cl_2$): $\tilde{\upsilon}/cm^{-1}$ = 1991s (t-CO), 1951s (t-CO), 1781m (μ-CO), 1691s (μ-CN)} and a minor amount of $[Fe_2Cp_2(CO)(CNPh)(\mu\text{-}CO)(\mu\text{-}CNPh)]$[54] {IR ($CH_2Cl_2$): $\tilde{\upsilon}/cm^{-1}$ = 2093s (t-CN)}. The solid (*ca* 0.8 mmol) was dissolved in anhydrous CH_2Cl_2 (15 mL) and methyl triflate (0.10 mL, 0.91 mmol) was added dropwise under stirring. The dark violet solution rapidly changed to dark red and was stirred at room temperature for 4 h. Next, the mixture was moved on top of an alumina column (h 4.5, d 4.5 cm). Impurities were eluted with CH_2Cl_2, CH_2Cl_2/THF 1:1 *v*/*v* and THF, then a red band was eluted with MeCN (*ca*. 200 mL). Volatiles were removed under vacuum. The residue was dissolved in CH_2Cl_2 and filtered over a celite pad. The filtrate solution was taken to dryness under vacuum, affording a red

foamy solid that was washed with hexane, dried under vacuum (40 °C) and stored under N_2. Yield: 194 mg, *ca*. 41 %. Soluble in CH_2Cl_2, acetone, EtOH, DMSO, scarcely soluble in Et_2O, toluene, insoluble in water. Anal. Calcd. for $C_{22}H_{18}F_3Fe_2NO_6S$: C, 44.55; H, 3.06; N, 2.36; S, 5.41. Found: C, 44.78; H, 3.20; N, 2.55; S, 5.24. IR (CH_2Cl_2): $\tilde{\upsilon}/cm^{-1}$ = 2025s (CO), 1993w-sh (CO), 1839m (μ-CO), 1549m, 1531w-sh (CN). ^1H NMR ($CDCl_3$): δ/ppm = 7.76 (br., 2H, Ph^{ortho}); 7.62 (t, $^3J_{HH}$ = 7.5 Hz, 2H, Ph^{meta}); 7.54 (t, $^3J_{HH}$ = 7.3 Hz, 1H, Ph^{para}); 5.43 (s, 5H, Cp); 4.72 (s, 5H, Cp'); 4.55 (s, 3H, Me). $^{13}C\{^1H\}$ NMR ($CDCl_3$): δ/ppm = 324.5 (μ-CN); 254.4 (μ-CO); 208.8, 207.7 (CO); 150.6 (Ph^{ipso}); 130.7 (Ph^{ortho}); 129.6 (Ph^{meta}); 125.3 (Ph^{para}); 120.9 (d, $^1J_{CF}$ = 309 Hz, CF_3); 90.5, 90.2 (Cp); 57.3 (Me). $^{19}F\{^1H\}$ NMR ($CDCl_3$): δ/ppm = − 78.0. The isolated compound contains *ca*. 7 % mol. of $[Fe_2Cp_2(CO)(CNPh)(\mu\text{-}CO)\{\mu\text{-}CN(Me)(Ph)\}]CF_3SO_3$. ^1H NMR ($CDCl_3$): δ/ppm = 7.48 (m), 7.10 (d) (Ph); 5.34 (s, 5H, Cp); 4.69 (s, 5H, Cp'); 4.55 (s, 3H, NMe). IR (CH_2Cl_2): $\tilde{\upsilon}/cm^{-1}$ = 2127 (t-CN), 1773 (μ-CO).

4. Isomerization reactions of [2]CF_3SO_3

General procedure. Complex **[2]CF_3SO_3** (*ca*. 15 mg) was heated at reflux under N_2 in selected solvents for several hours, then the solvent was removed under vacuum and the residue was analyzed by ^1H NMR ($CDCl_3$ solution). Thermal treatment in isopropanol, acetonitrile, methanol or toluene (1 to 4 hours) did not affect the isomeric ratio. Refluxing in DMF resulted in extensive degradation. Conditions leading to an increased isomeric ratio are reported in Table 5. Variable by-product formation and/or degradation was observed, generally more pronounced as the isomeric ratio increased.

Table 5. Experimental conditions and resulting isomeric ratios (evaluated by subsequent ^1H NMR spectra) related to **[2]CF_3SO_3**.

SOLVENT, TIME, TEMPERATURE	*CIS*/*TRANS* RATIO
ETOH, 4 H, REFLUX	6
ETOH, 7 H, REFLUX	8
ACETONE, 2.5 H, REFLUX	18

DMF, 4 H, 110 °C	9
DMF, OVERNIGHT, 110 °C	17

5. Electrochemistry

Cyclic voltammetry measurements were performed with a PalmSens4 instrument interfaced to a computer employing PSTrace5 electrochemical software. Anhydrous CH_2Cl_2 (Merck) and THF (Merck) were stored under argon over 3Å molecular sieves. $[N^nBu_4]PF_6$ (Fluka, electrochemical grade) and $FeCp_2$ (Fluka) were used without further purification. CV measurements were carried out under argon using 0.2 M $[N^nBu_4]PF_6$ in CH_2Cl_2 or THF as the supporting electrolyte. The working and the counter electrodes consisted of a Pt disk and a Pt gauze, respectively. A leakless miniature Ag/AgCl/KCl (3.4 mol/L) electrode (eDAQ) was employed as a reference. The three-electrode home-built cell was pre-dried by heating under vacuum and filled with argon. The Schlenk-type construction of the cell maintained anhydrous and anaerobic conditions. The solution of supporting electrolyte, prepared under argon, was introduced into the cell and the CV of the solvent was recorded. The analyte was then introduced and voltammograms were recorded; lastly, a small amount of ferrocene was added and the CV repeated. Under the present experimental conditions, the one-electron oxidation of ferrocene occurred at E° = +0.45 V *vs* Ag/AgCl in CH_2Cl_2, and at E° = +0.57 V *vs* Ag/AgCl in THF.

Phosphate buffer (PB) solution (Na_2HPO_4/KH_2PO_4, $\Sigma c_{(PO4)}$ = 50 mM, pH = 7.3) was prepared in ultrapure H_2O and used as aqueous supporting electrolyte. The three-electrode home-built cell was equipped with a Pt sheet counter electrode, teflon-encapsulated glassy-carbon (GC) working electrode (BASi, ø 3 mm) and the leak-free Ag/AgCl/KCl (3.4 mol/L) reference electrode (eDAQ). Prior to measurements, the working GC electrode was polished by the following procedure:[81] manual rubbing with 0.3 μM Al_2O_3 slurry in water (eDAQ) for 2 min, then sonication in ultrapure water for 10 min, manual rubbing with 0.05 μM Al_2O_3 slurry in water (eDAQ) for 2 min, then sonication in ultrapure water for 10 min. The PB (5.0 mL) was introduced into the cell, deaerated by argon bubbling for some minutes and the CV of the solvent recorded. The analyte was then introduced and voltammograms were

recorded (scan rate: 0.1 V/s). Under the present experimental conditions, the one-electron reduction of ferricinium in the PB occurred at E° = +0.20 V *vs* Ag/AgCl.

Controlled potential coulometry was performed in an H-shaped cell with anodic and cathodic compartments separated by a sintered-glass disk. The working macroelectrode and counter-electrode were platinum gauze.

Infrared (IR) spectroelectrochemical measurements were carried out using an optically transparent thin-layer electrochemical (OTTLE) cell equipped with CaF_2 windows, platinum mini-grid working and auxiliary electrodes and a silver wire pseudo-reference electrode.[59] During the microelectrolysis procedures, the electrode potential was controlled by a PalmSens4 instrument interfaced to a computer employing PSTrace5 electrochemical software. Argon-saturated CH_2Cl_2 or THF/$[N^nBu_4]PF_6$ 0.2 M solutions of the analyzed compound were used. The *in situ* spectroelectrochemical experiments were performed by collecting IR spectra at fixed time intervals during oxidation or reduction, obtained by continuously increasing or lowering the initial working potential at a scan rate of 1.0 or 2.0 $mV \cdot s^{-1}$, or by electrolysis at constant potential. In this second procedure, during the electrolysis the IR spectra were collected each 30 seconds.

6. DFT calculations

Geometry optimizations were performed using the PBEh-3c method, which is a reparametrized version of PBE0[82] (with 42% HF exchange) that uses a split-valence double-zeta basis set (def2-mSVP)[83,84] and adds three corrections considering dispersion, basis set superposition and other basis set incompleteness effects.[85,86,87] The C-PCM implicit solvation model was added to PBEh-3c calculations.[88,89] IR simulations were carried out using the harmonic approximation, from which zero-point vibrational energies and thermal corrections (T = 298.15 K) were obtained.[90] The software used was ORCA version 5.0.3.[91] The output was elaborated using MultiWFN, version 3.8.[92] Cartesian coordinates of the DFT-optimized structures are collected in a separated .xyz file.

7. Behavior in aqueous solutions

7.1 Solubility in D_2O. The selected diiron complex was suspended in a D_2O solution (0.7 mL) containing dimethyl sulfone (Me_2SO_2; $4.5 \cdot 10^{-3}$ M) and this suspension was stirred at room temperature (21±1 °C) for 3 h. The saturated solution was filtered over celite and analyzed by ^{1}H NMR (delay time = 3 s; number of scans = 20). The concentration (= solubility) was calculated as the relative integral with respect to Me_2SO_2 as internal standard [δ/ppm = 3.14 (s, 6H)] (Table 2). NMR data are reported in the Supporting Information.

7.2. Octanol/water partition coefficient (Log P_{ow}). Partition coefficients (P_{ow}), defined as $P_{ow} = c_{org}/c_{aq}$, where c_{org} and c_{aq} are the molar concentrations of the selected compound in the n-octanol and aqueous phase, respectively, were determined by the shake-flask method and UV-Vis measurements, according to a previously described procedure.[93,94] All operations were carried out at room temperature (21±1 °C). The stock solution of **[2]CF_3SO_3** was prepared in water-saturated octanol, while the stock solution of **[2]CF_3SO_3** in octanol-saturated water. The wavelength corresponding to a well-defined maximum of shoulder absorption of each compound (320–400 nm range) was used for UV-Vis quantitation. The procedure was repeated three times on each sample (from the same stock solution); results are given as mean ± standard deviation (Table 2).

7.3. Stability in CD_3OD/D_2O mixture. The selected diiron complex (*ca*. 5 mg) was dissolved in CD_3OD/D_2O (5:2 *v*/*v*, ca. 0.7 mL) containing $4.03 \cdot 10^{-3}$ M dimethylsulfone (Me_2SO_2) as internal standard. This solution was filtered over celite, then transferred into an NMR tube and the ^{1}H NMR spectrum was recorded. The mixture was maintained at 37 °C for 48 hours. After filtration over celite, the solution was analyzed by ^{1}H NMR. The residual amount of starting material in the final solution (with respect to the initial spectrum) was calculated as the relative integral with respect to Me_2SO_2 as internal standard. NMR spectra were recorded using the following settings: number of scans = 20; relaxation delay = 3 seconds. **[2]CF_3SO_3.** ^{1}H NMR (D_2O/CD_3OD 5/2 *v*/*v*): δ/ppm = 5.38, 5.31 (s, 5H);

4.94 (s,*), 4.80 (s,*), 4.78 (s,*); 4.60 (s), 4.57-4.54 (m), 4.51 (s) (7 H); *cis*/*trans* ratio ca. 1. *Over HDO peak. **[3]CF_3SO_3.** ^{1}H NMR (D_2O): δ/ppm = 7.74–7.62 (m, 5H), 5.44 (s, 5H), 4.55 (s, 3H). Cp' is hidden by HDO peak. ^{1}H NMR (D_2O/CD_3OD 5/2 *v*/*v*): δ/ppm = 7.85–7.59 (m, 5H), 5.46 (s, 5H), 4.78 (s), 4.56 (s, 3H).

7.4. Stability in CD_3OD/DMEM mixture. Deuterated cell culture medium (DMEM-d) was prepared by dissolving powdered DMEM cell culture medium (1000 mg/L glucose and L-glutamine, without sodium bicarbonate and phenol red; D2902 - Sigma Aldrich) in D_2O (10 mg/mL, according to the manufacturer's instructions). The solution was treated with Me_2SO_2 (*ca*. $6\cdot10^{-3}$ M), NaH_2PO_4 and Na_2HPO_4 (25 mM total phosphate, pD = 7.4)[95], then stored under N_2. Solutions of diiron complexes in a DMEM-d/CD_3OD 5/2 *v*/*v* mixture were prepared and treated as described above. The residual amount of starting material in solution after 24 h at 37 °C was calculated with respect to Me_2SO_2 as internal standard (Table 2).

8. Biological studies

8.1. Cytotoxicity

Tested complexes were dissolved in the minimum DMSO amount prior to cell culture testing. A calculated amount of the stock drug DMSO solution was added to the cell culture media to reach a final maximum DMSO concentration of 0.5%, which had no effects on cell viability. Cisplatin was dissolved in 0.9% sodium chloride solution. MTT [3-(4,5-dimethylthiazol-2-yl)- 2,5-diphenyltetrazolium bromide], cisplatin and ImmunoPure p-nitrophenyl phosphate (APH) were obtained from Sigma Chemical Co, St. Louis, USA.

8.2. Cell cultures. Human colon (HCT-15) and pancreatic (PSN-1) carcinoma cell lines along with human SCLC (U1285) were obtained from American Type Culture Collection (ATCC, Rockville, MD). Human ovarian 2008 cancer cells were kindly provided by Prof. G. Marverti (Dept. of

Biomedical Science of Modena University, Italy). Human cervical A431 cancer cells were kindly provided by Prof. P. Perego (Fondazione IRCCS Istituto Nazionale Tumori, Milan, Italy).

Cell lines were maintained in the logarithmic phase at 37°C in a 5% carbon dioxide atmosphere using RPMI-1640 culture medium containing 10% fetal calf serum (Euroclone, Milan, Italy), antibiotics (50 units/mL penicillin and 50 µg/mL streptomycin) and 2 mM l-glutamine.

8.3. Spheroid Cultures. Spheroid cultures were obtained by seeding 2.5 x 10^3 cells/well in round bottom non-tissue culture treated 96 well-plate (Greiner Bio-one, Kremsmünster, Austria) in phenol red free RPMI-1640 medium (Sigma Chemical Co.), containing 10% FCS and supplemented with 20% methyl cellulose stock solution.

8.4. MTT Assay. The growth inhibitory effect towards tumor cells was evaluated by means of MTT assay as previously described.[96] IC_{50} values were calculated with a four-parameter logistic (4-PL) model. All the values are the means ± SD of not less than four independent experiments.

8.5. Acid phosphatase (APH) assay. An APH modified assay was used for determining cell viability in 3D spheroids, as previously described.[97] IC_{50} values were calculated with a four-parameter logistic (4-PL) model. All the values are the means ± SD of not less than four independent experiments.

8.6. ROS Production. The production of ROS was measured in U1285 cells (10^4 per well) grown for 24 h in a 96-well plate in RPMI medium without phenol red (Sigma Chemical Co.). Cells were then washed with PBS and loaded with 10 µM 5-(and-6)-chloromethyl-2′,7′-dichlorodihydrofluorescein diacetate acetyl ester (CM–H_2DCFDA) (Molecular Probes-Invitrogen, Eugene, OR) for 25 min, in the dark. Afterwards, cells were washed with PBS and incubated with increasing concentrations of tested compounds. Fluorescence increase was estimated utilizing the wavelengths of 485 nm (excitation) and 527 nm (emission) in a VICTOR X3 (PerkinElmer, USA) plate reader. Antimycin (3 µM, Sigma Chemical Co), a potent inhibitor of Complex III in the electron transport chain, was used as positive control.

Conflicts of interest

There are no conflicts to declare.

Acknowledgements

L.B. and F.M. acknowledge the financial support from the University of Pisa (Fondi di Ateneo 2020).

Supporting Information Available

Synthesis/characterization of isocyanoferrocene; IR and NMR spectra; computational results; spectroelectrochemical studies. Cartesian coordinates of the DFT-optimized structures are collected in a separated .xyz file.

References

1 Astruc, D. Why is Ferrocene so Exceptional? *Eur. J. Inorg. Chem.* **2017**, 6–29.

2 Astruc, D. From sandwich complexes to dendrimers: journey toward applications to sensing, molecular electronics, materials science, and biomedicine, *Chem. Commun.* **2023**, *59*, 7321–7345.

3 Štěpnička, P. Forever young: the first seventy years of ferrocene, *Dalton Trans.* **2022**, *51*, 8085-8102.

4 van Staveren, D. R.; Metzler-Nolte, N. Bioorganometallic Chemistry of Ferrocene, *Chem. Rev.* **2004**, *104*, 5931–5986.

5 Patra, M.; Gasser, G. The medicinal chemistry of ferrocene and its derivatives, *Nat. Rev. Chem.* **2017**, *1*, 0066.

6 Boros, E.; Dyson, P. J.; Gasser, G. Classification of Metal-Based Drugs according to Their Mechanisms of Action, *Chem* **2020**, *6*, 41–60.

7 Anthony, E. J.; Bolitho, E. M.; Bridgewater, H. E.; Carter, O. W. L.; Donnelly, J. M.; Imberti, C.; Lant, E. C.; Lermyte, F.; Needham, R. J.; Palau, M.; Sadler, P. J.; Shi, H.; Wang, F.-X.; Zhang, W.-Y.; Zhang, Z.; Metallodrugs are unique: opportunities and challenges of discovery and development, *Chem. Sci.* **2020**, *11*, 12888–12917.

8 Atkinson, R. C. J.; Gibson, V. C.; Long, N. J. The syntheses and catalytic applications of unsymmetrical ferrocene ligands, *Chem. Soc. Rev.* **2004**, *33*, 313-328.

9 Array, R. G.; Adrio, J.; Carretero, J. C. Recent Applications of Chiral Ferrocene Ligands in Asymmetric Catalysis, *Angew. Chem. Int. Ed.* **2006**, *45*, 7674-7715.

10 Mu, C.; Chang, S. W.; Prosser, K. E.; Leung, A. W. Y.; Santacruz, S.; Jang, T.; Thompson, J. R.; Yapp, D. T. T.; Warren, J. J.; Bally, M. B.; Beischlag, T. V.; Walsby, C. J. Induction of Cytotoxicity in Pyridine Analogues of the Antimetastatic Ru(III) Complex NAMI - A by Ferrocene Functionalization, *Inorg. Chem.* **2016**, *55*, 177−190.

11 Gadre, S.; Manikandan, M.; Duari, P.; Chhatar, S.; Sharma, A.; Khatri, S.; Kode, J.; Barkume, M.; Kumar Kasinathan, N.; Nagare, M.; Patkar, M.; Ingle, A.; Kumar, M.; Kolthur-Seetharam, U.; Patra, M. A Rationally Designed Bimetallic Platinum (II)-Ferrocene Antitumor Agent Induces Non-Apoptotic Cell Death and Exerts in Vivo Efficacy, *Chem. Eur. J.* **2022**, *28*, e202201259.

12 López-Hernández, J. E.; Contel, M. Promising heterometallic compounds as anticancer agents: Recent studies in vivo, *Current Opinion Chem. Biol.* **2023**, *72*, 102250.

13 Mu, C.; Prosser, K. E.; Harrypersad, S.; MacNeil, G. A.; Panchmatia, R.; Thompson, J. R.; Sinha, S.; Warren, J. J.; Walsby, C. J. Activation by Oxidation: Ferrocene-Functionalized Ru(II)-Arene Complexes with Anticancer, Antibacterial, and Antioxidant Properties, *Inorg. Chem.* **2018**, *57*, 15247−15261.

14 Shubhankar Gadre, M. M.; Chhatar, S.; Chakraborty, G.; Ahmed, N.; Patra, C.; Patra, M. Potent Ruthenium–Ferrocene Bimetallic Antitumor Antiangiogenic Agent That Circumvents Platinum Resistance: From Synthesis and Mechanistic Studies to In Vivo Evaluation in Zebrafish, *J. Med. Chem.* **2022**, *65*, 16353–16371.

15 Tauchman, J.; Süss-Fink, G.; Stepnicka, P.; Zava, O.; Dyson, P. J. Arene ruthenium complexes with phosphinoferrocene amino acid conjugates: Synthesis, characterization and cytotoxicity, *J. Organomet. Chem.* **2013**, *723*, 233e238.

16 Carter, C.; Kratish, Y.; Jurca, T.; Gao, Y.; Marks, T. J. Bis-Ferrocenyl-Pyridinediimine Trinuclear Mixed-Valent Complexes with Metal-Binding Dependent Electronic Coupling: Synthesis, Structures, and Redox-Spectroscopic Characterization, *J. Am. Chem. Soc.* **2020**, *142*, 18715–18729.

17 Buday, P.; Celeda, M.; Görls, H.; Mlostoń, G.; Weigand, W. A Remarkable Ring Opening Observed in the Reaction of Cyclopropyl Ferrocenyl Thioketone with Triiron Dodecacarbonyl $Fe_3(CO)_{12}$, *Eur. J. Inorg. Chem.* **2022**, e202200520.

18 Camara, J. M.; Rauchfuss, T. B. Combining acid–base, redox and substrate binding functionalities to give a complete model for the [FeFe]-hydrogenase, *Nat. Chem.* **2012**, *4*, 26-30.

19 Marchetti, F. Constructing Organometallic Architectures from Aminoalkylidyne Diiron Complexes, *Eur. J. Inorg. Chem.* **2018**, 3987–4003.

20 Ritleng, V.; Chetcuti, M. J. Hydrocarbyl Ligand Transformations on Heterobimetallic Complexes, *Chem. Rev.* **2007**, *107*, 797−858.

21 van Beek, C. B.; van Leest, N. P.; Lutz, M.; de Vos, S. D.; Klein Gebbink, R. J. M.; de Bruin, B.; Broere, D. L. J. Combining metal–metal cooperativity, metal–ligand cooperativity and chemical non-innocence in diiron carbonyl complexes, *Chem. Sci.* **2022**, *13*, 2094 – 2104.

22 Biancalana, L.; Marchetti, F. Aminocarbyne ligands in organometallic chemistry, *Coord. Chem. Rev.* **2021**, *449*, 214203.

23 Agonigi, G.; Biancalana, L.; Lupo, M. G.; Montopoli, M.; Ferri, N.; Zacchini, S.; Binacchi, F.; Biver, T.; Campanella, B.; Pampaloni, G.; Zanotti, V.; Marchetti, F. Exploring the Anticancer Potential of Diiron Bis-

cyclopentadienyl Complexes with Bridging Hydrocarbyl Ligands: Behavior in Aqueous Media and In Vitro Cytotoxicity, *Organometallics* **2020**, *39*, 645 – 657.

24 Biancalana, L.; De Franco, M.; Ciancaleoni, G.; Zacchini, S.; Pampaloni, G.; Gandin, V.; Marchetti, F. Easily Available, Amphiphilic Diiron Cyclopentadienyl Complexes Exhibit in vitro Anticancer Activity in 2D and 3D Human Cancer Cells through Redox Modulation Triggered by CO Release, *Chem. Eur. J.* **2021**, *27*, 10169–10185.

25 Campanella, B.; Braccini, S.; Bresciani, G.; De Franco, M.; Gandin, V.; Chiellini, F.; Pratesi, A.; Pampaloni, G.; Biancalana, L.; Marchetti, F. The choice of μ-vinyliminium ligand substituents is key to optimize the antiproliferative activity of related diiron complexes, *Metallomics* **2023**, mfac096.

26 Rocco, D.; Batchelor, L. K.; Agonigi, G.; Braccini, S.; Chiellini, F.; Schoch, S.; Biver, T.; Funaioli, T.; Zacchini, S.; Biancalana, L.; Ruggeri, M.; Pampaloni, G.; Dyson, P. J.; Marchetti, F. Anticancer potential of diiron vinyliminium complexes, *Chem. Eur. J.* **2019**, *25*, 14801-14816.

27 Bresciani, B.; Cervinka, J.; Kostrhunova, H.; Biancalana, L.; Bortoluzzi, M.; Pampaloni, G.; Novohradsky, V.; Brabec, V.; Marchetti, F.; Kasparkova, J. N-Indolyl diiron vinyliminium complexes exhibit antiproliferative effects in cancer cells associated with disruption of mitochondrial homeostasis, ROS scavenging, and antioxidant activity, *Chemico-Biological Interactions* **2023**, *385*, 110742.

28 Schoch, S.; Braccini, S.; Biancalana, L.; Pratesi, A.; Funaioli, T.; Zacchini, S.; Pampaloni, G.; Chiellini, F.; Marchetti, F. When ferrocene and diiron organometallics meet: triiron vinyliminium complexes exhibit strong cytotoxicity and cancer cell selectivity, *Inorg. Chem. Front.* **2022**, *9*, 5118-5139.

29 According to IUPAC, metal complexes comprising a carbyne ligand should be called "alkylidyne" complexes. See: F. R. KreiBl in “Transition Metal Carbyne Complexes”, Ed. Springer **1993**. However, the term “aminocarbyne” is more familiar in the literature than “aminoalkylidyne”, and the former will be preferentially used throughout this manuscript.

30 Willis, S.; Manning, A. R. Reactions of $[Fe_2(\eta\text{-}C_5H_5)_2(CO)_{4-n}(CNR)_n]$ (n= 1 or 2; R = Me, Et, or CH2Ph) with acetyl and benzoyl chlorides, *J. Chem. Soc., Dalton Trans.* **1981**, 322–324.

31 Complexes $[Fe_2Cp_2(CO)_2(\mu\text{-}CO)\{\mu\text{-}CN(Me)(R)\}]CF_3SO_3$ (R = ^{t}Bu, 4-C_6H_4CN) largely decompose upon passing through an alumina column; using a procedure analogous to that illustrated in Scheme 1, the formation of complexes with R = 2,6-$C_6H_4F_2$ and R = CH_2SO_2(4-C_6H_4Me) did not occur, even when the CO-substitution step was conducted at reflux temperature.

32 Pombeiro, A. J. L.; Guedes da Silva, M. F. C.; Michelin, R. A. Aminocarbyne complexes derived from isocyanides activated towards electrophilic addition, *Coord. Chem. Rev*. **2001**, *218*, 43–74.

33 Biancalana, L.; Ciancaleoni, G.; Zacchini, S.; Pampaloni, G.; Marchetti, F. Carbonyl-isocyanide mono-substitution in $[Fe_2Cp_2(CO)_4]$: A re-visitation, *Inorg. Chim. Acta* **2020**, *517*, 120181, and references therein.

34 Barybin, M. V. Nonbenzenoid aromatic isocyanides: New coordination building blocks for organometallic and surface chemistry, *Coord. Chem. Rev.* **2010**, *254*, 1240–1252.

35 Nemykin, V. N.; Dudkin, S. V.; Spaeth, A. D.; Rhoda, H. M.; Belosludov, R. V.; Barybin, M. V. Probing Electronic Communications in Heterotrinuclear Fe − Ru – Fe Molecular Wires Formed by Ruthenium(II) Tetraphenylporphyrin and Isocyanoferrocene or 1,1′-Diisocyanoferrocene Ligands, *Inorg. Chem.* **2015**, *54*, 10711−10724.

36 Nemykin, V. N.; Purchel, A. A.; Spaeth, A. D.; Barybin, M. V. Probing the Electronic Properties of a Trinuclear Molecular Wire Involving Isocyanoferrocene and Iron(II) Phthalocyanine Motifs, *Inorg. Chem.* **2013**, *52*, 11004 – 11012.

37 Huang, Y.-C.; Lan, W.-Y.; Ching, W.-M.; Hsu, S. C. N. Formation of iron(III)–thiolate metallocyclophane using a ferrocene-based bis-isocyanide, *New J. Chem.* **2020**, *44*, 18242—18249.

38 Barybin, M. V.; Holovics, T. C.; Deplazes, S. F.; Lushington, G. H.; Powell, D. R.; Toriyama, M. First Homoleptic Complexes of Isocyanoferrocene, *J. Am. Chem. Soc*. **2002**, *124*, 13668 – 13669.

39 Vosahlo, P.; Franc, M.; Harmach, P.; Schulz, J.; Stepnicka, P. Synthesis of gold(I) diaminocarbene complexes by the addition of amines across coordinated isocyanoferrocene, *J. Organomet. Chem.* **2023**, *1001*, 122843

40 Mahmudov, K. T.; Kukushkin, V. Yu.; Gurbanov, A. V.; Kinzhalov, M. A.; Boyarskiy, V. P.; Guedes da Silva, M. F. C.; Pombeiro, A. J .L. Isocyanide metal complexes in catalysis, *Coord. Chem. Rev.* **2019**, *384*, 65–89.

41 Boyarskiy, V. P.; Bokach, N. A.; Luzyanin, K. V.; Kukushkin, V. Yu. Metal-Mediated and Metal-Catalyzed Reactions of Isocyanides, *Chem. Rev*. **2015**, *115*, 2698 – 2779.

42 Biancalana, L.; Fiaschi, M.; Ciancaleoni, G.; Pampaloni, G.; Zanotti, V.; Zacchini, S.; Marchetti, F. A comparative structural and spectroscopic study of diiron and diruthenium isocyanide and aminocarbyne complexes, *Inorg. Chim. Acta* **2022**, *536*, 120886.

43 Guillevic, M. A.; Hancox, E. L.; Mann, B. E. A Reinvestigation of the Solution Structure and Dynamics of $[Fe_2(\eta^5\text{-}C_5H_5)_2(CO)_{4-n}(CNMe)_n]$, n = 1 or 2, *J. Chem. Soc. Dalton Trans*. **1992**, 1729-1733.

44 Farrugia, L. J. Dynamics and fluxionality in metal carbonyl clusters: some old and new problems, *J. Chem. Soc., Dalton Trans.* **1997**, *11*, 1783–1792.

45 Howell, J. A. S.; Rowan, A. J. Synthesis and fluxional character of complexes of the type $[M_2(cp)_2(CO)_3(CNR)]$(M = Fe or Ru, cp =η-C_5H_5), *J. Chem. Soc., Dalton Trans*. **1980**, *3*, 503–510.

46 Burrows, A. D.; Fleischer, H.; Mingos, D. M. P. The synthesis and structural characterization of a pentapalladium cluster, $[Pd_5(\mu\text{-}SO_2)_3(\mu\text{-}CNXyl)_2(CNXyl)_5]$, with linear bridging isocyanide ligands, *J. Organomet. Chem.* **1992**, *433*, 311-321.

47 Agonigi, G.; Bortoluzzi, M.; Marchetti, F.; Pampaloni, G.; Zacchini, S.; Zanotti, V. Regioselective Nucleophilic Additions to Diiron Carbonyl Complexes Containing a Bridging Aminocarbyne Ligand: A Synthetic, Crystallographic and DFT Study, *Eur. J. Inorg. Chem.* **2018**, 960–971.

48 Cox, G.; Dowling, C.; Manning, A. R.; McArdle, P.; Cunningham, D. A reinvestigation of the reaction of $[Fe_2(\eta\text{-}C_5H_5)_2(CO)_{4-n}(CNR)_n]$ (n = 1 or 2) with strong alkylating agents, *J. Organomet. Chem.* **1992**, *438*, 143-158.

49 Pombeiro, A. J. L. Electron-donor/acceptor properties of carbynes, carbenes, vinylidenes, allenylidenes and alkynyls as measured by electrochemical ligand parameters, *J. Organomet. Chem.* **2005**, *690*, 6021–6040.

50 Bresciani, G.; Zacchini, S.; Pampaloni, G.; Bortoluzzi, M.; Marchetti, F. Diiron Aminocarbyne Complexes with NCE^- Ligands (E = O, S, Se), *Molecules* **2023**, *28*, 3251.

51 Hu, H.; Ichiryu, H.; Nakajima, K.; Ogasawara, M. Estimating Effective Steric and Electronic Impacts of a Ferrocenyl Group in Organophosphines, *ACS Omega* **2021**, *6*, 5981-5989.

52 Hill, A. F.; Manzano, R. A. A [C_1 + C_2] route to propargylidyne complexes, *Dalton Trans.* **2019**, *48*, 6596-6610.

53 Howell, J. A. S.; Mays, M. J.; Hunt, I. D.; Mills, O. S. The preparation and structural characterization of anti-di-μ-phenylisonitrile-trans-dicarbonylbis(η-cyclopentadienyl)diiron, *J. Organomet. Chem.* **1977**, *128*, C29-C30.

54 Manning, A. R.; McNally, G.; Soye, P. The preparation and spectra of $[Fe_2(\eta\text{-}C_5H_5)_2(CO)_{4\text{-}n}(CNAr)_n]$ complexes. The reaction of $[Fe(CO)_{5\text{-}m}(CNAr)_m]$ with dicyclopentadiene, *Inorg. Chim. Acta* **1991**, *180*, 103-110.

55 Joshi, K. K.; Mills, O. S.; Pauson, P. L.; Shaw, B. W.; Stubbs, W. H. An Iron Complex with a Bridging Isonitrile Group, *Chem. Comm.* **1965**, *10*, 181-182.

56 Christian, G.; Lentz, D.; Hartl, H.; Fehlhammer, W. P. Di- und Trieisenkomplexe mit funktionellen Isocyanidbrucken, *Chem. Ber.* **1992**, *125*, 1093-1100.

57 Gorelsky, S. I.; Ghosh, S.; Solomon, E. I. Mechanism of N_2O Reduction by the μ^4-S Tetranuclear Cu Z Cluster of Nitrous Oxide Reductase, *J. Am. Chem. Soc.* **2006**, *128*, 278-290.

58 Mazzoni, R.; Gabiccini, A.; Cesari, C.; Zanotti, V.; Gualandi, I.; Tonelli, D. Diiron complexes bearing bridging hydrocarbyl ligands as electrocatalysts for proton reduction, *Organometallics* **2015**, *34*, 3228–3235.

59 Krejčik, M.; Daněk M.; Hartl, F. Simple construction of an infrared optically transparent thin-layer electrochemical cell: Applications to the redox reactions of ferrocene, $Mn_2(CO)_{10}$ and $Mn(CO)_3$(3,5-di-t-butyl-catecholate), *J. Electroanal. Chem.* **1991**, *317*, 179–187.

60 Fabrizi de Biani, F.; Ienco, A.; Laschi, F.; Leoni, P.; Marchetti, F.; Marchetti, L.; Mealli, C.; Zanello, P. Formation and Characterization of the Hexanuclear Platinum Cluster $[Pt_6(\mu\text{-}PBu^t_2)_4(CO)_6](CF_3SO_3)_2$ through Structural, Electrochemical, and Computational Analyses, *J. Am. Chem. Soc.* **2005**, *127*, 3076–3089.

61 Arrigoni, F.; Bertini, L.; De Gioia, L.; Cingolani, A.; Mazzoni, R.; Zanotti, V.; Zampella, G. Mechanistic Insight into Electrocatalytic H_2 Production by $[Fe_2(CN)\{\mu\text{-}CN(Me)_2\}(\mu\text{-}CO)(CO)(Cp)_2]$: Effects of Dithiolate Replacement in [FeFe] Hydrogenase Models, *Inorg. Chem.* **2017**, *56*, 13852−13864.

62 Hillard, E. A.; Caxico de Abreu, F.; Melo Ferreira, D. C.; Jaouen, G.; Oliveira Fonseca Goulart, M.; Amatore, C. Electrochemical parameters and techniques in drug development, with an emphasis on quinones and related compounds, *Chem. Commun.* **2008**, 2612-2628.

63 Reisner, E.; Arion, V. B.; Guedes da Silva, M. F. C.; Lichtenecker, R.; Eichinger, A.; Keppler, B. K.; Kukushkin, V. Yu.; Pombeiro, A. J. L. Tuning of Redox Potentials for the Design of Ruthenium Anticancer Drugs – an Electrochemical Study of [*trans*-$RuCl_4L(DMSO)]^-$ and [*trans*-$RuCl_4L_2]^-$ Complexes, where L = Imidazole, 1,2,4-Triazole, Indazole, *Inorg. Chem.* **2004**, *43*, 7083–7093.

64 Kirlin, W. G.; Cai, J.; Thompson, S. A.; Diaz, D. Glutathione Redox Potential in Response to Differentiation and Enzyme Inducers, *Free Radical Biol. Med.* **1999**, *27*, 1208–1218.

65 In both cases, water/CD_3OD mixtures (5:2 v/v) were used to achieve a concentration of the diiron compound which is appropriate for ^1H NMR.

66 Compound [**3**]CF_3SO_3 resulted significantly less active than [**2**]CF_3SO_3 in terms of IC_{50} data ROS production (*vide infra*). Therefore, it is reasonable to neglect the influence of the $[Fe_2Cp_2(CO)(CNPh)(\mu\text{-}CO)\{\mu\text{-}CN(Me)(Ph)\}]^+$ by-product on the biological data of [**3**]CF_3SO_3.

67 Kunz-Schughart, L.A.; Freyer, J.P.; Hofstaedter, F.; Ebner, R. T J. The use of 3-D cultures for high-throughput screening: the multicellular spheroid model, *Biomol. Screen.* **2004**, *9*, 273–285.

68 Menges, F. "Spectragryph - optical spectroscopy software", Version 1.2.16.1 @2016-2022 http://www.effemm2.de/spectragryph.

69 Fulmer, G. R.; Miller, A. J. M.; Sherden, N. H.; Gottlieb, H. E.; Nudelman, A.; Stoltz, B. M.; Bercaw, J. E.; Goldberg, K. I. NMR Chemical Shifts of Trace Impurities: Common Laboratory Solvents, Organics, and Gases in Deuterated Solvents Relevant to the Organometallic Chemist, *Organometallics* **2010**, *29*, 2176–2179.

70 Willker, W.; Leibfritz, D.; Kerssebaum, R.; Bermel, W. Gradient selection in inverse heteronuclear correlation spectroscopy, *Magn. Reson. Chem.* **1993**, *31*, 287-292.

71 Holovics, T. C.; Deplazes, S. F.; Toriyama, M.; Powell, D. R.; Lushington, G. H.; Barybin, M. V. Organometallic Isocyanocyclopentadienides: A Combined Synthetic, Spectroscopic, Structural, Electrochemical and Theoretical Investigation, *Organometallics* **2004**, *23*, 2927-2938.

72 Sethi, S.; Das, P. K.; Behera, N. The chemistry of aminoferrocene, $Fe\{(\eta^5\text{-}C_5H_4NH_2)(Cp)\}$: Synthesis, reactivity and applications, *J. Organomet. Chem.* **2014**, *824*, 140-165.

73 Weber, W. P.; Gokel, G. W.; Ugi, I. K. Phase Transfer Catalysis in the Hofmann Carbylamine Reaction, *Angew. Chem. Int. Ed.* **1972**, *11*, 530-531.

74 Kim, B.; Beebe, J. M.; Jun, Y.; Zhu, X.-Y.; Frisbie, C. D. Correlation between HOMO Alignment and Contact Resistance in Molecular Junctions: Aromatic Thiols versus Aromatic Isocyanides, *J. Am. Chem. Soc.* **2006**, *128*, 4970–4971.

75 Zakrzewski, J.; Krawczyk, M. Synthesis and Pesticidal Properties of Thio and Seleno Analogs of Some Common Urea Herbicides, *Phosphorus Sulfur Silicon Relat. Elem.* **2009**, *184*, 1880–1903.

76 Dhake, K. P.; Tambade, P. J.; Singhal, R. S.; Bhanage, B. M. An efficient, catalyst- and solvent-free N-formylation of aromatic and aliphatic amines, *Green Chem. Lett. Rev.* **2011**, *4*, 151-157

77 Lacerda, R. B.; de Lima, C. K. F.; da Silva, L. L.; Romeiro, N. C.; Miranda, A. L. P.; Barreiro, E. J.; Fraga, C. A. M. Discovery of novel analgesic and anti-inflammatory 3-arylamine-imidazo[1,2-a]pyridine symbiotic prototypes, *Bioorg. Med. Chem.* **2009**, *17*, 74–84.

78 Leifert, D.; Artiukhin, D. G.; Neugebauer, J.; Galstyan, A.; Strassert, C. A.; Studer, A. Radical perfluoroalkylation – easy access to 2-perfluoroalkylindol-3-imines via electron catalysis, *Chem. Commun.* **2016**, *52*, 5997-6000.

79 Skoch, K.; Cisarova, I.; Stepnicka, P. Selective Gold-Catalysed Synthesis of Cyanamides and 1-Substituted 1H-Tetrazol-5-Amines from Isocyanides, *Chem. Eur. J.* **2018**, *24*, 13788-13791.

80 Howell, J. A. S.; Matheson, T. W.; Mays, M. J. Carbon-13 Nuclear Magnetic Resonance Studies of Isonitrile Derivatives of Tetracarbonylbis-(η-cyclopentadienyl)di-iron, *J. Chem. Soc. Chem. Comm.* **1975**, 865-866.

81 Gross, M.; Jordan, J. Voltammetry At Glassy Carbon Electrodes, *Pure & Appl. Chem.* **1984**, *56*, 1095-1129.

82 Grimme, S.; Brandenburg, J. G.; Bannwarth, C.; Hansen, A. A. Consistent structures and interactions by density functional theory with small atomic orbital basis sets, *J. Chem. Phys.* **2015**, *143*, 054107.

83 Weigend, F.; Ahlrichs, R. Balanced basis sets of split valence, triple zeta valence and quadruple zeta valence quality for H to Rn: Design and assessment of accuracy, *Phys. Chem. Chem. Phys.* **2005**, *7*, 3297–3305.

84 Weigend, F. Accurate Coulomb-fitting basis sets for H to Rn, *Phys. Chem. Chem. Phys.* **2006**, *8*, 1057–1065.

85 Kruse, H.; Grimme, S. A geometrical correction for the inter- and intra-molecular basis set superposition error in Hartree-Fock and density functional theory calculations for large systems, *J. Chem. Phys.* **2012**, *136*, 154101.

86 Grimme, S.; Ehrlich, S.; Goerigk, L. Effect of the damping function in dispersion corrected density functional theory, *J. Comput. Chem.* **2011**, *32*, 1456–1465.

87 Grimme, S.; Antony, J.; Ehrlich, S.; Krieg, H. A consistent and accurate ab initio parametrization of density functional dispersion correction (DFT-D) for the 94 elements H-Pu, *J. Chem. Phys.* **2010**, *132*, 154104.

88 Cossi, M.; Rega, N.; Scalmani, G.; Barone, V. Energies, structures, and electronic properties of molecules in solution with the C-PCM solvation model, *J. Comput. Chem.* **2003**, *24*, 669–681.

89 Barone, V.; Cossi, M.; Quantum Calculation of Molecular Energies and Energy Gradients in Solution by a Conductor Solvent Model, *J. Phys. Chem. A* **1998**, *102*, 1995–2001.

90 Cramer, C. J. Essentials of Computational Chemistry, 2nd ed.,Wiley, Chichester, **2004**.

91 Neese, F. Software update: The ORCA program system - Version 5.0, WIREs *Comput. Mol. Sci.* **2022**, e1616.

92 Lu, T.; Chen, F.; A Multifunctional Wavefunction Analyzer, *J. Comput. Chem.* **2012**, *33*, 580–592.

93 Dearden, J. C.; Bresnen, G. M. Quant. Struct.-Act. Relat. **1988**, *7*, 133-144.

94 Bresciani, G.; Busto, N. V. Ceccherini, M. Bortoluzzi, G. Pampaloni, B. Garcia, F. Marchetti, Screening the biological properties of transition metal carbamates reveals gold(I) and silver(I) complexes as potent cytotoxic and antimicrobial agents, *J. Inorg. Biochem.* **2022**, *227*, 111667.

95 Calculated by the formula pD = pH* + 0.4, where pH* is the value measured for H2O-calibrated pH-meter; (a) Westcott, C. C. pH Measurements; Academic Press: New York, **1978**. (b) Covington, A. K.; Paabo, M.; Robinson, R. A.; Bates. R. G. *Anal. Chem.* **1968**, *40*, 700-706.

96 Harper, B. W. J.; Petruzzella, E.; Sirota, R.; Faccioli, F.F.; Aldrich-Wright, J. R.; Gandin, V.; Gibson, D.; Synthesis, characterization and in vitro and in vivo anticancer activity of Pt(iv) derivatives of [Pt(1S,2S-DACH)(5,6-dimethyl-1,10-phenanthroline)], *Dalton Trans*. **2017**, *46*, 7005-7019.

97 Gandin, V.; Ceresa, C.; Esposito, G.; Indraccolo, S.; Porchia, M.; Tisato, F.; Santini, C.; Pellei, M.; Marzano, C. Therapeutic potential of the phosphino Cu(I) complex (HydroCuP) in the treatment of solid tumors, *Sci Rep.* **2017**, *7*, 13936.